Environmental Science & Technology Letters

Letter

Cite This: Environ. Sci. Technol. Lett. 2019, 6, 205−210

pubs.acs.org/journal/estlcu

Molecular Initiating Events of Bisphenols on Androgen Receptor-Mediated Pathways Provide Guidelines for *in Silico* Screening and Design of Substitute Compounds

Qinchang Chen,[†] Xiaoxiang Wang,[†] Haoyue Tan,[†] Wei Shi,*[,†] Xiaowei Zhang,[†] Si Wei,[†] John P. Giesy,[†,‡,§,∥] and Hongxia Yu[†]

[†]State Key Laboratory of Pollution Control and Resources Reuse, School of the Environment, Nanjing University, Nanjing, Jiangsu 210023, People's Republic of China

[‡]Department of Veterinary Biomedical Sciences and Toxicology Centre, University of Saskatchewan, Saskatoon, SK S7N 5B3, Canada

[§]Department of Zoology and Center for Integrative Toxicology, Michigan State University, East Lansing, Michigan 48824, United States

[∥]Department of Environmental Science, Baylor University, Waco, Texas 76798, United States

Supporting Information

ABSTRACT: Bisphenols (BPs) have the potential to interfere with the androgen receptor (AR). However, *in silico* screening and substitute design were difficult because little was known about the mechanisms by which BPs interfere with AR-mediated molecular initiating events (MIEs). Here, the AR disrupting effects and associated mechanisms of 15 BPs were evaluated by *in vitro* assays and molecular dynamics simulations. AR-mediated MIEs, including ligand−receptor interactions and coregulator recruitment, might determine active versus inactive and agonist versus antagonist activities of BPs, respectively. Bisphenol E (BPE), BPF, and BPS with no binding effects were inactive, while all other BPs were AR antagonists. On the basis of their coregulator recruitment patterns and repositioning of helix 12, BPBP, BPC, and BPPH were passive antagonists that blocked coregulator recruitment, and their anti-androgenic potencies were correlated with ligand−receptor interactions; others were active antagonists that recruited corepressors, and their anti-androgenic potencies were correlated with ligand−receptor−corepressor interactions. A new method was developed for MIE-based *in silico* qualitative and quantitative evaluations of the potential of BPs to disrupt AR-mediated pathways, by which safer BPA substitutes with smaller and less hydrophobic connecting groups could be designed. The MIE-based *in silico* methods can be used to screen a wider range of chemicals and to design better substitutes.

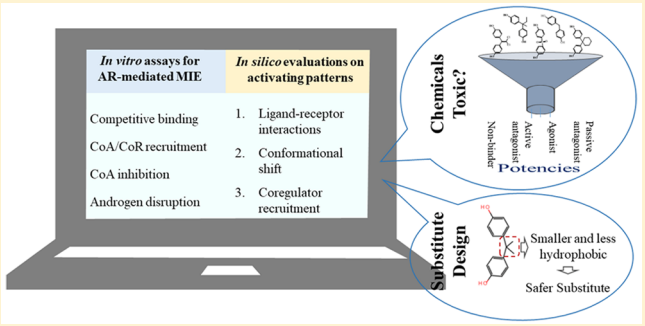

INTRODUCTION

Bisphenol A (BPA) is one of the most well-known bisphenols (BPs) and one of the most produced chemicals in the world. BPA is widely used in manufacturing and is ubiquitous in the environment.[1] Because of the growing concern about the endocrine disrupting effects of BPA,[2,3] some other BPs, including BPAF, BPAP, BPF, and BPS, are now being used as substitutes for BPA. These widely used substitutes are detectable in various products, even in those labeled as a BPA-free product.[4−6]

According to adverse outcome pathways (AOPs),[7] activation of the androgen receptor (AR) (https://aopwiki.org/aops/23) is an important molecular initiating event (MIE) that triggers the AOP and results in adverse outcomes (AOs). Some BPs have been reported to disrupt activation of the AR and cause anti-androgenic effects, while some BPs, such as BPAF and BPCH, are more potent disruptors than BPA.[8,9] However, AR disrupting potencies of most BPs were not tested, which makes the evaluation of AR disrupting potencies of BPs an urgent need to avoid their substitution with more potent BPs. Nevertheless, *in vivo/vitro* assays are expensive and time-consuming and when performed with humans have ethical limitations, and epidemiological assessments of associations are compromised by confounding factors, including exposures to other chemicals. Computer-based methods, being high-throughput for chemical evaluation, offer a robust and economical option for efficiently evaluating

Received: February 15, 2019
Revised: March 11, 2019
Accepted: March 13, 2019
Published: March 13, 2019

DOI: 10.1021/acs.estlett.9b00073
Environ. Sci. Technol. Lett. 2019, 6, 205−210

chemicals.[10] However, previous models recognized the importance of only ligand−receptor interactions for the activation of the AR, which failed to predict chemicals to be inactive, agonists or antagonists. Because the functioning of chemicals is dependent on activation of an MIE,[11] classification of structurally different BPs according to mechanisms of action of AR-mediated MIEs is necessary to screen their AR disrupting potencies.

Similar to the scarcity of data with regard to the abilities of BPs to disrupt AR-mediated pathways, mechanisms by which structurally different BPs interfere with activation of the AR remained unknown, which limited the development of *in silico* screening and design of better substitutes in green chemistry. To the best of our knowledge, BPs have the potential to activate AR-mediated MIEs by three biochemical processes: ligand binding/unbinding, conformational shifts, and coregulator recruitment (Figure S1).[12,13] Molecular simulations have shown their potential for use in investigating ligand−receptor interactions, protein−protein interactions, and conformational shifts in previous studies,[14−16] which might aid in our understanding of mechanisms of action of BPs interfering with AR-mediated MIEs. The use of *in silico* methods in toxicology embraces ideas similar to those of green chemistry.[17] Molecular mechanisms derived from molecular simulations are conducive to *in silico* screening of potential androgen disrupting chemicals, which can reduce the use of *in vivo* assays,[18] and molecular and atomic interactions derived from molecular simulations assist with the design of safer BPA substitutes.[19]

In this study, results of androgen disruption, competitive binding, and coregulator recruitment derived from *in vitro* assays and details of ligand−receptor and ligand−receptor−coregulator interactions derived from molecular simulations were combined to provide insights into how 15 BPs bind to AR and activate the AR-mediated MIE. On the basis of these data, activating patterns and relevant AR disrupting potencies of BPs were correlated. Furthermore, a computational method for MIE-based *in silico* screening was developed, and a method for designing BPA substitutes based on key interactions between BPs and AR was developed.

MATERIALS AND METHODS

Materials. Structures and chemical information for all tested chemicals are presented in Figure S2 and Table S1. The 15 BPs (>98% pure) were purchased from AccuStandard. The AR agonist 5α-dihydrotestosterone (DHT; >99.5% pure) was purchased from Dr. Ehrenstorfer-Schäfers's laboratory, and the AR antagonist flutamide (FT; >99% pure) from Sigma-Aldrich. All chemicals were dissolved in dimethyl sulfoxide (DMSO) and stored at −20 °C.

Cell Culture and Reporter Gene Assays. The MDA-kb2 cell line[20] was cultured in Leibowitz-15 (L15) medium supplemented with 10% fetal bovine serum (FBS) and used charcoal dextran-stripped FBS instead for experiments. Detailed descriptions of the assays are provided in the Supporting Information. Briefly, the cells were seeded in a 384-well plate, and the DMSO content was maintained at <0.1% (v/v) after exposure. Cell viabilities were tested and chemicals were diluted according to their cytotoxicities (Figure S4A). MDA-kb2 cells were exposed to dilutions of chemicals with or without 1×10^{-9} M DHT (~EC_{80} in the reporter gene assay) to assess anti-androgenic or androgenic potencies. Dose−response curves for DHT and FT (Figure S4B) indicated the reliability of the reporter gene assays.

Competitive Binding Assays. AR competitive binding assays were performed using a PolarScreen kit (Thermo Fisher), following the protocol provided by the manufacturer. Three concentrations were tested for DHT, FT, and BPs, and the DMSO content was maintained 1% (v/v).

TR-FRET Coregulator Assays. Coregulator recruitment assays were performed using LanthaScreen TR-FRET kits (Thermo Fisher) following the protocol provided by the manufacturer. For coactivator inhibition assays, BPs with 5×10^{-8} M DHT (~EC_{80} in the coactivator recruitment assay) were added individually to the assay system. Three concentrations were tested for each compound, and the DMSO content was maintained at 1% (v/v).

Molecular Dynamics (MD) Simulations. The preparation of chemical structures and AR-LBD was performed according to previously described methods.[15] MD and steered MD (SMD) simulations were performed using GROMACS version 5.12.[21,22] MD simulations of ligand−receptor interactions, conformational shifts, and coregulator recruitment were performed as follows. (1) Ligand−receptor interactions were investigated by ligand binding and unbinding processes, by using MD simulations, molecular mechanics Poisson−Boltzmann surface area (MM-PBSA) binding free energies,[23] and SMD simulations. (2) Conformational shifts were analyzed on the basis of trajectories of MD simulations, and snapshots of equilibrated conformations were extracted to determine the modes of helix 12 (H12) repositioning. (3) Coregulator recruitment was evaluated by use of protein docking,[15] followed by MD simulations, binding free energy calculations, and SMD simulations of the ligand−receptor−coregulator complexes. Details of the structure preparation, molecular docking, MD simulations, MM-PBSA binding free energy calculations, SMD simulations, and protein docking are described in the Supporting Information.

Data Analysis. Results of *in vitro* assays were analyzed using GraphPad Prism 6.01 and are presented as the mean ± standard error (SE) of more than three independent experiments. Multiple comparisons were calculated using one-way analysis of variance plus Dunnett post-test correction, with p values ≤0.05 considered to be significant. All dose−response curves were derived by use of a model (eq 1).

$$Y = \text{Bottom} + \frac{\text{Top} - \text{Bottom}}{1 + 10^{(\log \text{IC}_{\text{Median}} - x)\text{Hill slope}}} \quad (1)$$

where IC_{Median} is the concentration (molar) of the chemical that gives a response halfway between Bottom and Top and the Hill slope is the steepness of the curve. Anti-androgenic potencies were derived as RIC_{20} (the concentration showing 20% inhibition of luciferase activity induced by 1×10^{-9} M DHT) of BPs and are presented as logarithm values. Principal component analyses (PCAs) of the binding and unbinding results were performed using KNIME version 3.3.2,[24] and the first component was considered as a ligand−receptor interaction score (LRI_{score}).

RESULTS AND DISCUSSION

Androgen Disruptions of BPs in the Reporter Gene Assays. On the basis of the results of reporter gene assays, 12 of 15 BPs (Figure S5) exhibited measurable anti-androgenic potencies, among which anti-androgenic effects of BPA, BPAF,

DOI: 10.1021/acs.estlett.9b00073
Environ. Sci. Technol. Lett. 2019, 6, 205−210

Table 1. Results of the *in Vitro* Assays and the Molecular Simulations[a]

	in vitro					*in silico*						
chemical	log RIC_{20}	bind	CoA	CoR	CoA_{inh}	$\Delta G_{lig\text{-}recep}$	unbinding path	PF_{mini}	LRI_{score}	helix 12 mode	activity category	predicted potency
BPA	−5.70	+	+	++	−	−86.52	path 4	1.19×10^3	−0.53	S	active antagonist	−5.81
BPAF	−7.10	+	++	+++	−	−107.44	path 4	1.37×10^3	0.46	S	active antagonist	−7.32
BPAP	−7.12	+	+++	++	−	−110.98	path 4	2.28×10^3	1.83	S	active antagonist	−6.90
BPBP	−6.16	+	−	−	++	−109.81	path 1	1.32×10^3	0.46	B	passive antagonist	−6.08
BPC	−5.75	+	−	−	+	−107.86	path 2	5.16×10^2	−0.71	B	passive antagonist	−5.79
BPC2	−6.37	++	+	+	−	−96.38	path 4	1.73×10^3	0.55	S	active antagonist	−5.99
BPE	ND[b]	−				−88.99	path 4	5.13×10^2	−1.38		inactive	
BPF	ND	−				−78.70	path 4	5.11×10^2	−1.75		inactive	
BPG	−6.77	+	+	+	+	−125.53	path 4	7.76×10^2	0.27	S	active antagonist	−6.63
BPM	−6.40	+	++	+++	−	−129.20	path 4	6.24×10^2	0.19	S	active antagonist	−6.52
BPP	−5.80	+	++	+	−	−114.94	path 4	5.10×10^2	−0.47	S	active antagonist	−6.22
BPPH	−6.38	+	−	−	+	−146.93	path 1	1.36×10^3	1.83	B	passive antagonist	−6.42
BPS	ND	−				−79.08	path 4	4.93×10^2	−1.76		inactive	
BPTMC	−6.99	++	++	++	+	−122.26	path 4	1.15×10^3	0.67	S	active antagonist	−6.93
BPZ	−7.21	+	++	+++	−	−113.21	path 4	9.06×10^2	0.02	S	active antagonist	−7.14
DHT		+++	+++	−	−	−141.51	path 3	1.10×10^3	1.28	A	agonist	
FT		+	+	+++	+	−98.80	path 3	5.67×10^2	−0.96	S	active antagonist	

[a]Values of log RIC_{20} are logarithms of the concentration (molar) showing 20% inhibition of luciferase activity induced by 1×10^{-9} M DHT. Bind indicates results from the competitive binding assays. CoA, CoR, and CoA_{inh} are the results from coactivator recruitment, corepressor recruitment, and coactivator inhibition assays, respectively. Values of $\Delta G_{lig\text{-}recep}$ are binding free energies of ligands with AR (kilojoules per mole). The unbinding path indicates the pathway that requires the least pulling force to unbind from AR. PF_{mini} is the peak of the pulling force (kilojoules per mole per nanometer) along the pathway with the least pulling force. LRI_{score} is the ligand−receptor interaction score. The number of plus signs represents the number of concentrations among the three tested concentrations (concentrations of the BPs and FT were 4×10^{-6}, 2×10^{-5}, and 1×10^{-4} M, and concentrations of DHT were 4×10^{-8}, 2×10^{-7}, and 1×10^{-6} M) showing a significant difference. A minus sign means no significant difference was observed. [b]ND = not detected.

BPC, and BPZ were consistent with results of previous studies.[8,9,25,26] In contrast, none of the BPs showed androgenic effects. Three BPs, including BPE, BPF, and BPS, were inactive in reporter gene assays, a result that is consistent with results of previous studies.[8,25] Three-quarters of the tested BPs used in manufacturing were more potent androgen disruptors than BPA (log RIC_{20} = −5.70), among which BPZ (log RIC_{20} = −7.21) was the most potent, calling into question their use as substitutes for BPA. To avoid more toxic BPs and to design safer substitutes, how BPs interact with the AR at a molecular level must be understood to be able to develop *in silico* screening methods for evaluating the potential disruption of BPA substitutes.

Binding and Unbinding between BPs and AR: Key Features for Androgen Disruption. Competitive binding assays indicated that BPA, BPAF, BPZ, and the other nine BPs, as well as DHT and FT, were avid binders to the AR whereas BPE, BPF, and BPS were nonbinders (Table 1). These results were consistent with those of previous studies.[8,27] Considering only AR binders induced anti-androgenic effects in the reporter gene assays, it was apparent that disruptions of AR-mediated pathways were a function of binding and unbinding processes.

The strength of binding can be evaluated by the use of free energies of binding [$\Delta G_{lig\text{-}recep}$ (Table 1)]. Greater free energies of binding demonstrate weaker binding potencies of the BP−AR complexes. The $\Delta G_{lig\text{-}recep}$ of BPA (−86.52 kJ/mol) indicated a relatively weak association with AR. BPF and BPS were the only two BPs with $\Delta G_{lig\text{-}recep}$ values greater than that of BPA. These weaker affinities of binding would result in inadequate interactions with AR but were not sufficient to exclude nonbinders (Table 1). Results of several studies of nuclear receptors have demonstrated four major pathways of unbinding (Figure S6A,B).[28,29] Peaks of pulling forces (PFs), which are forces needed for ligands to break interactions with the AR during SMD simulations[29,30] (Figure S6C,D), indicated that 12 of 15 BPs were more likely to dissociate along pathway 4 (Table 1 and Table S2). Ligand dissociation is the breaking of multiple short-range, noncovalent bonds included in ligand−receptor interactions,[31] which has been considered to be an important feature for MD simulations of NRs.[32,33] However, previous studies provided subjective comparisons that remain controversial when considering more than one unbinding pathway.[34] Pulling forces from SMD simulations indicated the major unbinding pathway of BPs and made quantitative descriptions possible.

Binding and unbinding processes were integrated [LRI_{score} (Table 1)] to comprehensively score ligand−AR interactions, which revealed that results of MD simulations agreed with those of *in vitro* assays. A greater LRI_{score} indicated more potential for interacting with the AR. Via comparison of results of MD simulations with competitive binding assays,[8,27] BPE, BPF, and BPS with the lowest LRI_{score} were the only chemicals determined to be nonbinders (Figure S6E), which were also inactive in the reporter gene assays. It was indicated that binding and unbinding processes were key features of BP−AR interactions, and evaluating the BP−AR interactions by exploring both binding and unbinding processes allows characterizations of inactive chemicals. These results were then confirmed because nonbinders were also determined to be inactive in transactivation reporter gene assays.

Coregulator Recruitment Influenced by BPs: Activating Patterns of AR. Results of TR-FRET assays revealed that patterns of coregulator recruitment were influenced by BPs (Table 1). The agonist DHT caused recruitment of the coactivator (CoA) but not the corepressor (CoR), whereas nine BPs, including BPA and BPAF, caused recruitment of

DOI: 10.1021/acs.estlett.9b00073
Environ. Sci. Technol. Lett. 2019, 6, 205−210

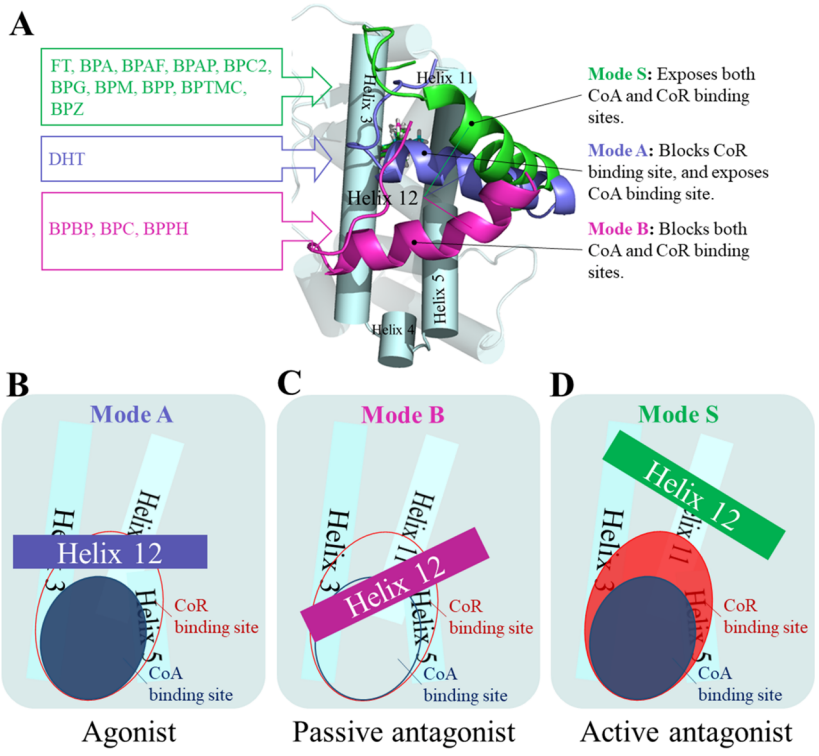

Figure 1. Three modes of helix 12 repositioning. (A) Equilibrated helix 12 (H12) of BPC, DHT, and BPZ-bound androgen receptor (AR) that represent modes B, A, and S of H12 repositions, respectively, which are colored hot pink, purple, and green, respectively. Helices 1−11 are colored light cyan. (B−D) Coregulator binding sites and their relationship with helix 12 repositioning of modes A, B, and S, respectively, which result in agonist, passive antagonist, and active antagonist, respectively. Coactivator and corepressor binding sites are depicted as the blue and red ellipses, respectively.

both CoA and CoR, which is similar to the case of antagonist FT. These results agreed with those observed during a previous study that BPA and BPAF caused AR to recruit both CoA and CoR.[35] The other three BPs, BPBP, BPC, and BPPH, inhibited recruitment of CoA during co-exposure with DHT. Therefore, the agonistic effect of DHT could result from exclusive recruitment of CoA, and antagonistic effects of BPs could result from either recruitment of CoR or inhibition of CoA recruitment. The influence of repositioning of H12 and associated coregulator recruitment confirmed this assumption.

Results of MD simulations indicated modes A, B, and S of H12 repositioning (Figure 1 and Table 1). H12 of mode A blocks the CoR binding site and exposes the CoA binding site (Figure 1A,B). H12 of mode B blocks both CoA and CoR binding sites (Figure 1A,C). H12 of mode S exposed both binding sites of CoA and CoR (Figure 1A,D).[12] H12 of DHT-AR was classified as mode A, which agreed with coregulator recruitment patterns and was consistent with crystal structures of DHT-AR (Figure S8).[36,37] BPBP, BPC, and BPPH caused mode B repositioning (Figure 1 and Table 1), which resulted in blocking of both CoA and CoR. The other nine BPs induced mode S, which resulted in recruitment of either CoA or CoR, and were indicated to bind CoR stronger than CoA using protein docking (Figure S9). Although the antagonistic form of the crystal structure of AR is not yet clear, the blocked conformations and the corepressor-bound conformations derived from MD simulations are comparable with crystal structures of other antagonist-bound steroid hormone receptors.[38−40] Therefore, results of conformational shift and coregulator recruitment derived from MD simulations were consistent with results of coregulator recruitment assays and their antagonistic effects. BPBP, BPC, and BPPH inducing mode B repositioning were classified as passive antagonists that inhibited CoA to cause antagonism, whereas BPA, BPAF, BPAP, BPC2, BPG, BPM, BPP, BPTMC, and BPZ inducing mode S repositioning were active antagonists that recruited CoR to result in antagonism (Table 1 and Figure S8).[41]

Potencies of BPs to disrupt AR-mediated pathways could not be correlated by simply using ligand−receptor interactions [$\Delta G_{lig\text{-}recep}$, PF, or LRI_{score}, all $R^2 \leq 0.304$ (Figures S10 and S11A)]. This phenomenon can be attributed to shifts in the conformation of AR and coregulator recruitment because different patterns of coregulator recruitment resulted in different patterns of AR activation, which are dependent on various interactions. Although there were only three passive antagonists, because their mechanism of action was to keep the ligand−AR complexes away from coregulators (Figure S11A), anti-androgenic potency correlated well with the ligand−receptor interaction score. In contrast, for active antagonists, because their mechanism of action was to recruit CoR and interact with the ligand, receptor, and CoR, anti-androgenic potencies were correlated with LRI_{score} and CoR binding free energies [R^2 = 0.820 (Figure S11B and Table S3)]. Together, predicted anti-androgenic potencies for active and passive antagonists had a coefficient of determination (R^2) of 0.859 (Figure S10C). Furthermore, recruitment of CoR might be more important than ligand−receptor interactions in determining anti-androgenic potencies of active antagonists. This implies that the influence of CoR was indispensable in predicting anti-androgenic potencies.

Potential Application of the AR-Mediated MIE: Computer-Aided Green Chemistry. Having characterized

DOI: 10.1021/acs.estlett.9b00073
Environ. Sci. Technol. Lett. 2019, 6, 205−210

mechanisms by which BPs initiated AR-mediated MIE at both functional and structural levels, using both *in vitro* and *in silico* methods, we reasoned that molecular simulations could aid in the interpretation of AR-mediated MIE and development of MIE-based *in silico* screening of environmental pollutants. A workflow for MIE-based *in silico* screening was developed (Figure S12) to evaluate influences of chemicals on nuclear receptors. Ligand−receptor interactions revealed by binding and unbinding processes assist with screening of nonbinders that are inactive. According to the repositioning of H12 and subsequent coregulator recruitment, chemicals can be qualitatively categorized as agonists, passive antagonists, and active antagonists. Quantitative prediction was further performed on the basis of interactions among mechanisms of action. By using this workflow, the *in silico* screening procedure of endocrine disrupting chemicals mediated by nuclear receptors, such as AR, ER, GR, and mineralocorticoid receptor (MR), could be developed. The application of such predictive models to evaluate a wider range of chemicals might curtail the use of *in vitro* and *in vivo* tests.

BPs are structurally similar compounds (Figure S2), which are mainly different in the connecting group (CG) (except BPC and BPG). BPs bound to AR in a similar binding mode (Figure S13), and CGs interacted mainly with residues on H8 and H11. Lu et al. innovatively used fluorescence spectroscopy and MD simulation to provide perspective information about safer bisphenol substitutes.[16] In this study, by use of free energy decomposition, four residues (Met780, Met787, Phe876, and Leu880) on H8 and H11 were found to be the key residues (Table S4).[42,43] Ligand−receptor interactions were found to correlate with free energy contributions of all four key residues [R^2 = 0.724 (Figure S14)], which indicated that interactions between CGs and these residues were key interactions for ligand−receptor interactions. Because Met780, Met787, Phe876, and Leu880 were hydrophobic residues, BPs of less hydrophobic and smaller CGs (Table S4) would result in weaker ligand−AR interactions. Therefore, BPs with the smallest and least hydrophobic CGs as possible would be preferred as potential BPA substitutes to reduce the influence on AR-mediated MIE. These rules could benefit the design of BPA substitutes with weaker AR disrupting effects, and this workflow can be extended to other nuclear receptors or to the design of safer substitutes for other chemicals.

■ ASSOCIATED CONTENT

Supporting Information

The Supporting Information is available free of charge on the ACS Publications website at DOI: 10.1021/acs.estlett.9b00073.

Additional details about methods and discussions, Figures S1−S14, and Tables S1−S4 (PDF)

■ AUTHOR INFORMATION

Corresponding Author

*E-mail: njushiwei@nju.edu.cn.

ORCID

Qinchang Chen: 0000-0001-9793-8676
Wei Shi: 0000-0001-9499-818X
Xiaowei Zhang: 0000-0001-8974-9963
Si Wei: 0000-0002-5868-4332

Notes

The authors declare no competing financial interest.

■ ACKNOWLEDGMENTS

This work was supported by the National Key R&D Program of China (2018YFC1801604), the Natural Science Foundation of China (21577058), the Science Fund for Excellent Young Scholars of Jiangsu Province (BK20170077), and the National Water Pollution Control and Treatment Science and Technology Major Project (2017ZX07202-001 and 2017ZX07602-002). The computational calculations were performed in the High Performance Computing Center (HPCC) of Nanjing University and the National Supercomputing Center in Shenzhen.

■ REFERENCES

(1) Rubin, B. S. Bisphenol A: An Endocrine Disruptor with Widespread Exposure and Multiple Effects. *J. Steroid Biochem. Mol. Biol.* **2011**, *127*, 27−34.

(2) Brown, J. S. Effects of Bisphenol-A and Other Endocrine Disruptors Compared with Abnormalities of Schizophrenia: An Endocrine-Disruption Theory of Schizophrenia. *Schizophr. Bull.* **2009**, *35*, 256−278.

(3) Usman, A.; Ahmad, M. From BPA to Its Analogues: Is It a Safe Journey? *Chemosphere* **2016**, *158*, 131−142.

(4) Rochester, J. R.; Bolden, A. L. Bisphenol S and F: A Systematic Review and Comparison of the Hormonal Activity of Bisphenol a Substitutes. *Environ. Health Perspect.* **2015**, *123*, 643−650.

(5) Liao, C.; Kannan, K. A Survey of Alkylphenols, Bisphenols, and Triclosan in Personal Care Products from China and the United States. *Arch. Environ. Contam. Toxicol.* **2014**, *67*, 50−59.

(6) Cunha, S. C.; Cunha, C.; Ferreira, A. R.; Fernandes, J. O. Determination of Bisphenol A and Bisphenol B in Canned Seafood Combining QuEChERS Extraction with Dispersive Liquid-Liquid Microextraction Followed by Gas Chromatography-Mass Spectrometry. *Anal. Bioanal. Chem.* **2012**, *404*, 2453−2463.

(7) Ankley, G. T.; Bennett, R. S.; Erickson, R. J.; Hoff, D. J.; Hornung, M. W.; Johnson, R. D.; Mount, D. R.; Nichols, J. W.; Russom, C. L.; Schmieder, P. K.; et al. Adverse Outcome Pathways: A Conceptual Framework to Support Ecotoxicology Research and Risk Assessment. *Environ. Toxicol. Chem.* **2010**, *29*, 730−741.

(8) U.S. Environmental Protection Agency. iCSS ToxCast Dashboard. https://actor.epa.gov/dashboard/.

(9) Kitamura, S.; Suzuki, T.; Sanoh, S.; Kohta, R.; Jinno, N.; Sugihara, K.; Yoshihara, S.; Fujimoto, N.; Watanabe, H.; Ohta, S. Comparative Study of the Endocrine-Disrupting Activity of Bisphenol A and 19 Related Compounds. *Toxicol. Sci.* **2005**, *84*, 249−259.

(10) Raunio, H. In Silico Toxicology − Non-Testing Methods. *Front. Pharmacol.* **2011**, *2*, 00033.

(11) Browne, P.; Noyes, P. D.; Casey, W. M.; Dix, D. J. Application of Adverse Outcome Pathways to U.S. EPA's Endocrine Disruptor Screening Program. *Environ. Health Perspect.* **2017**, *125*, 096001.

(12) Chen, Q.; Tan, H.; Yu, H.; Shi, W. Activation of Steroid Hormone Receptors: Shed Light on the in Silico Evaluation of Endocrine Disrupting Chemicals. *Sci. Total Environ.* **2018**, *631−632*, 27−39.

(13) Gronemeyer, H.; Gustafsson, J. Å.; Laudet, V. Principles for Modulation of the Nuclear Receptor Superfamily. *Nat. Rev. Drug Discovery* **2004**, *3*, 950−964.

(14) Wang, X.; Yang, H.; Hu, X.; Zhang, X.; Zhang, Q.; Jiang, H.; Shi, W.; Yu, H. Effects of HO-/MeO-PBDEs on Androgen Receptor: In Vitro Investigation and Helix 12-Involved MD Simulation. *Environ. Sci. Technol.* **2013**, *47*, 11802−11809.

(15) Chen, Q.; Wang, X.; Shi, W.; Yu, H.; Zhang, X.; Giesy, J. P. Identification of Thyroid Hormone Disruptors among HO-PBDEs: In Vitro Investigations and Coregulator Involved Simulations. *Environ. Sci. Technol.* **2016**, *50*, 12429−12438.

DOI: 10.1021/acs.estlett.9b00073
Environ. Sci. Technol. Lett. 2019, 6, 205−210

(16) Lu, L.; Zhan, T.; Ma, M.; Xu, C.; Wang, J.; Zhang, C.; Liu, W.; Zhuang, S. Thyroid Disruption by Bisphenol S Analogues via Thyroid Hormone Receptor B: In Vitro, in Vivo, and Molecular Dynamics Simulation Study. *Environ. Sci. Technol.* **2018**, *52*, 6617−6625.
(17) Maertens, A.; Anastas, N.; Spencer, P. J.; Stephens, M.; Goldberg, A.; Hartung, T. Green Toxicology. *ALTEX* **2014**, *31*, 243−249.
(18) Gramatica, P.; Cassani, S.; Sangion, A. Aquatic Ecotoxicity of Personal Care Products: QSAR Models and Ranking for Prioritization and Safer Alternatives' Design. *Green Chem.* **2016**, *18*, 4393−4406.
(19) Bharatham, N.; Finch, K. E.; Min, J.; Mayasundari, A.; Dyer, M. A.; Guy, R. K.; Bashford, D. Performance of a Docking/Molecular Dynamics Protocol for Virtual Screening of Nutlin-Class Inhibitors of Mdmx. *J. Mol. Graphics Modell.* **2017**, *74*, 54−60.
(20) Wilson, V. S.; Bobseine, K.; Lambright, C. R.; Gray, L. E. A Novel Cell Line, MDA-Kb2, That Stably Expresses an Androgen- and Glucocorticoid-Responsive Reporter for the Detection of Hormone Receptor Agonists and Antagonists. *Toxicol. Sci.* **2002**, *66*, 69−81.
(21) Pronk, S.; Pall, S.; Schulz, R.; Larsson, P.; Bjelkmar, P.; Apostolov, R.; Shirts, M. R.; Smith, J. C.; Kasson, P. M.; van der Spoel, D.; et al. GROMACS 4.5: A High-Throughput and Highly Parallel Open Source Molecular Simulation Toolkit. *Bioinformatics* **2013**, *29*, 845−854.
(22) Abraham, M. J.; Murtola, T.; Schulz, R.; Páll, S.; Smith, J. C.; Hess, B.; Lindahl, E. Gromacs: High Performance Molecular Simulations through Multi-Level Parallelism from Laptops to Supercomputers. *SoftwareX* **2015**, *1*−*2*, 19−25.
(23) Kumari, R.; Kumar, R.; Lynn, A. G-Mmpbsa: A GROMACS Tool for High-Throughput MM-PBSA Calculations. *J. Chem. Inf. Model.* **2014**, *54*, 1951−1962.
(24) Berthold, M. R.; Cebron, N.; Dill, F.; Gabriel, T. R.; Kötter, T.; Meinl, T.; Ohl, P.; Thiel, K.; Wiswedel, B. KNIME - the Konstanz Information Miner. *ACM SIGKDD Explor. Newsl.* **2009**, *11*, 26.
(25) Teng, C.; Goodwin, B.; Shockley, K.; Xia, M.; Huang, R.; Norris, J.; Merrick, B. A.; Jetten, A. M.; Austin, C. P.; Tice, R. R. Bisphenol A Affects Androgen Receptor Function via Multiple Mechanisms. *Chem.-Biol. Interact.* **2013**, *203*, 556−564.
(26) Rosenmai, A. K.; Dybdahl, M.; Pedersen, M.; Alice van Vugt-Lussenburg, B. M.; Wedebye, E. B.; Taxvig, C.; Vinggaard, A. M. Are Structural Analogues to Bisphenol a Safe Alternatives? *Toxicol. Sci.* **2014**, *139*, 35−47.
(27) Fang, H.; Tong, W.; Branham, W. S.; Moland, C. L.; Dial, S. L.; Hong, H.; Xie, Q.; Perkins, R.; Owens, W.; Sheehan, D. M. Study of 202 Natural, Synthetic, and Environmental Chemicals for Binding to the Androgen Receptor. *Chem. Res. Toxicol.* **2003**, *16*, 1338−1358.
(28) Martínez, L.; Webb, P.; Polikarpov, I.; Skaf, M. S. Molecular Dynamics Simulations of Ligand Dissociation from Thyroid Hormone Receptors: Evidence of the Likeliest Escape Pathway and Its Implications for the Design of Novel Ligands. *J. Med. Chem.* **2006**, *49*, 23−26.
(29) Shen, J.; Li, W.; Liu, G.; Tang, Y.; Jiang, H. Computational Insights into the Mechanism of Ligand Unbinding and Selectivity of Estrogen Receptors. *J. Phys. Chem. B* **2009**, *113*, 10436−10444.
(30) Lüdemann, S. K.; Lounnas, V.; Wade, R. C. How Do Substrates Enter and Products Exit the Buried Active Site of Cytochrome P450cam? 2. Steered Molecular Dynamics and Adiabatic Mapping of Substrate Pathways. *J. Mol. Biol.* **2000**, *303*, 813−830.
(31) Danilowicz, C.; Greenfield, D.; Prentiss, M. Dissociation of Ligand-Receptor Complexes Using Magnetic Tweezers. *Anal. Chem.* **2005**, *77*, 3023−3028.
(32) Mackinnon, J. A. G.; Gallastegui, N.; Osguthorpe, D. J.; Hagler, A. T.; Estébanez-Perpiñá, E. Allosteric Mechanisms of Nuclear Receptors: Insights from Computational Simulations. *Mol. Cell. Endocrinol.* **2014**, *393*, 75−82.
(33) Wu, Y.; Doering, J. A.; Ma, Z.; Tang, S.; Liu, H.; Zhang, X.; Wang, X.; Yu, H. Identification of Androgen Receptor Antagonists: In Vitro Investigation and Classification Methodology for Flavonoid. *Chemosphere* **2016**, *158*, 72−79.
(34) Renaud, J. P.; Rochel, N.; Ruff, M.; Vivat, V.; Chambon, P.; Gronemeyer, H.; Moras, D. Crystal Structure of the RAR-Gamma Ligand-Binding Domain Bound to All-Trans Retinoic Acid. *Nature* **1995**, *378*, 681−689.
(35) Perera, L.; Li, Y.; Coons, L. A.; Houtman, R.; van Beuningen, R.; Goodwin, B.; Auerbach, S. S.; Teng, C. T. Binding of Bisphenol A, Bisphenol AF, and Bisphenol S on the Androgen Receptor: Coregulator Recruitment and Stimulation of Potential Interaction Sites. *Toxicol. In Vitro* **2017**, *44*, 287−302.
(36) Nadal, M.; Prekovic, S.; Gallastegui, N.; Helsen, C.; Abella, M.; Zielinska, K.; Gay, M.; Vilaseca, M.; Taulès, M.; Houtsmuller, A. B.; et al. Structure of the Homodimeric Androgen Receptor Ligand-Binding Domain. *Nat. Commun.* **2017**, *8*, 14388.
(37) Zhou, X. E.; Suino-Powell, K. M.; Li, J.; He, Y.; MacKeigan, J. P.; Melcher, K.; Yong, E. L.; Xu, H. E. Identification of SRC3/AIB1 as a Preferred Coactivator for Hormone-Activated Androgen Receptor. *J. Biol. Chem.* **2010**, *285*, 9161−9171.
(38) Schoch, G. A.; D'Arcy, B.; Stihle, M.; Burger, D.; Bär, D.; Benz, J.; Thoma, R.; Ruf, A. Molecular Switch in the Glucocorticoid Receptor: Active and Passive Antagonist Conformations. *J. Mol. Biol.* **2010**, *395*, 568−577.
(39) Shiau, A. K.; Barstad, D.; Loria, P. M.; Cheng, L.; Kushner, P. J.; Agard, D. A.; Greene, G. L. The Structural Basis of Estrogen Receptor/Coactivator Recognition and the Antagonism of This Interaction by Tamoxifen. *Cell* **1998**, *95*, 927−937.
(40) Madauss, K. P.; Grygielko, E. T.; Deng, S.-J.; Sulpizio, A. C.; Stanley, T. B.; Wu, C.; Short, S. A.; Thompson, S. K.; Stewart, E. L.; Laping, N. J.; et al. A Structural and in Vitro Characterization of Asoprisnil: A Selective Progesterone Receptor Modulator. *Mol. Endocrinol.* **2007**, *21*, 1066−1081.
(41) Shiau, A. K.; Barstad, D.; Radek, J. T.; Meyers, M. J.; Nettles, K. W.; Katzenellenbogen, B. S.; Katzenellenbogen, J. A.; Agard, D. A.; Greene, G. L. Structural Characterization of a Subtype-Selective Ligand Reveals a Novel Mode of Estrogen Receptor Antagonism. *Nat. Struct. Biol.* **2002**, *9*, 359−364.
(42) Liu, H.; Han, R.; Li, J.; Liu, H.; Zheng, L. Molecular Mechanism of R-Bicalutamide Switching from Androgen Receptor Antagonist to Agonist Induced by Amino Acid Mutations Using Molecular Dynamics Simulations and Free Energy Calculation. *J. Comput.-Aided Mol. Des.* **2016**, *30*, 1189−1200.
(43) Bohl, C. E.; Wu, Z.; Miller, D. D.; Bell, C. E.; Dalton, J. T. Crystal Structure of the T877A Human Androgen Receptor Ligand-Binding Domain Complexed to Cyproterone Acetate Provides Insight for Ligand-Induced Conformational Changes and Structure-Based Drug Design. *J. Biol. Chem.* **2007**, *282*, 13648−13655.

DOI: 10.1021/acs.estlett.9b00073
Environ. Sci. Technol. Lett. 2019, 6, 205−210

Supporting Information

Molecular Initiating Events of Bisphenols on AR-Mediated Pathways Provide Guidelines for *In Silico* Screening and Design of Substitute Compounds

Qinchang Chen[†], Xiaoxiang Wang[†], Haoyue Tan[†], Wei Shi[†, *], Xiaowei Zhang[†], Si Wei[†], John P. Giesy[†, ‡, §, ǁ], Hongxia Yu[†]

[†] State Key Laboratory of Pollution Control and Resources Reuse, School of the Environment, Nanjing University, Nanjing, Jiangsu 210023, People's Republic of China

[‡] Department of Veterinary Biomedical Sciences and Toxicology Centre, University of Saskatchewan, Saskatoon, SK S7N 5B3, Canada.

[§] Department of Zoology, and Center for Integrative Toxicology, Michigan State University, East Lansing, MI 48824, USA

[ǁ]Department of Environmental Science, Baylor University, Waco, TX 76798, USA

***Corresponding Author:**

Wei Shi: njushiwei@nju.edu.cn

Supporting Methods

Hypothesis about AR-mediated MIE

Results of previous studies have indicated activation of AR-mediated MIE includes three important biochemical processes (Figure S1).[1,2] Molecular dynamics (MD) simulation was used to determine if activation by BPs follows this classical mode: 1) ligand binding to and interacts with AR, which is considered to be the most important for the activation of AR-mediated MIE; 2) Conformation of AR shifts as a result of interaction between the ligand and the AR, which results in a significant repositioning of helix 12 (H12); and 3) coregulator recruitment is facilitated or blocked by repositioning of H12, which results in activation or repression of transcription. Recruitment of coactivator (CoA) facilitates binding of other transcription factors and acetylates the DNA, which promotes transcription and induced agonistic effect. Conversely, the recruitment of corepressor (CoR) results in the deacetylation of target DNA, which leads to repression of transcription, which is called an "active antagonist" effect.[3] If AR fails to recruit either a CoA or a CoR, transcription will be interrupted, which results in a "passive antagonist" effect.[3]

Cell culture and reporter gene assays

The MDA-kb2 cell line, which is stably transfected with a luciferase reporter gene driven by an androgen-response element-containing promoter,[4] was cultured in Leibowitz-15 (L15) medium (Gibco, Invitrogen Corporation, Carlsbad, CA, USA) and was supplemented with 10% fetal bovine serum (FBS; Gibco) at 37 °C in a humidified atmosphere without additional CO_2. L15 medium with 10% charcoal-dextran-stripped FBS (CDS-FBS; Gibco) was used instead of the standard culture medium 24 hours before the cells were seeded to a 384-well white opaque plate (Corning Inc., Corning, NY, USA) at a density of 1×10^5 cells/mL. After chemical exposure, the final volume of

assay media was 80 μL/well, and DMSO content was maintained at less than 0.1% (v/v). Prior to androgenic and anti-androgenic tests, one solution cell proliferation assays (MTS) were performed to assess the viabilities of all chemicals using CellTiter 96® AQueous One Solution Cell Proliferation Assay Kit (Promega, Madison, WI, USA), and chemicals were diluted according to their cytotoxicities. Based on viabilities of cells exposed to various BPs (Figure S4A), to avoid cytotoxicities, a maximum concentration of BPs, of 4 μM was employed in assays to determine agonistic and antagonistic potencies. MDA-kb2 cells were exposed to dilutions of chemicals with or without 1×10^{-9} M DHT to assess anti-androgenic or androgenic potencies. After 24 hours of exposure, the medium was removed and 10 μL of 1 × lysis buffer (Promega) was pipetted into each well. After 10 min of cell lysis, 25 μL of luciferase reagent (Promega) was pipetted into each well. Luciferase activity was recorded immediately by use of a Synergy H4 microplate reader (BioTek, Winooski, VT, USA). DHT and FT were used as positive controls for androgenic and anti-androgenic effects, respectively.

Mechanism-based molecular simulations

MD simulations of ligand-receptor interactions, conformational shift and coregulator recruitment were performed as follows: (1) Ligand-receptor interactions were investigated by ligand binding and unbinding processes, by using MD simulations, molecular mechanics Poisson-Boltzmann surface area (MM-PBSA) binding free energies[5] and SMD simulations. One hundred snapshots from the MD trajectories of each complex were extracted for calculations of binding free energy using the g_mmpbsa package [5] that was developed from the GROMACS and APBS [6] programs. A velocity of 1 nm/ns was used during 3-ns SMD simulations, and the harmonic force constant was set at 1000 $\mathrm{kJ\cdot mol^{-1}nm^{-2}}$. The details of the MD simulations, binding free energies

calculations and SMD simulations are described in the following.

(2) Conformational shift was analyzed based on trajectories of MD simulations. Root-mean-square deviations (RMSD) of MD trajectories were calculated to evaluate the conformational equilibration of complexes. Modes of H12 repositioning were determined based on snapshots of equilibrated conformations.

(3) Coregulator recruitment was evaluated by use of protein docking following the previously described method.[7] Corepressor (PDB code: 2JFA) and coactivator (PDB code: 3L3X) motifs were pre-positioned on the coregulator binding surface according to the previous publications. Hex 8.0.0,[13] a protein docking program, was used to modify the positions of coregulators and give a shape-based docking score E_{dock}. Coregulators were then docked to the extracted complexes using shape-based 3D fast Fourier transform (FFT) docking methods. The receptor and ligand range angles were all set to 15 degrees to make sure the co-regulators did not rotate far away from the reference positions. Ligand-receptor-coregulator complexes derived from protein docking were used to perform MD simulations and binding free energy calculations, followed by SMD simulations to investigate the ligand-receptor-coregulator interactions.

Structure preparation and molecular docking

Structures of the tested chemicals were built according to the NCBI PubChem Compound (http://www.ncbi.nlm.nih.gov/pccompound).Structural energy minimization was then carried out to optimize the geometries using Powell gradient algorithm and the Tripos force field[8] by the Minimize module interfaced with SYBYL7.3 (Tripos Inc., St. Louis, MO, USA). Gasteiger-Huckel charges were also added to the structures.

Structure of androgen receptor (AR) ligand binding domain (LBD) was built by homology

modeling using Swiss-Model[9,10] online modeling system (http://swissmodel.expasy.org/). Crystal structure of DHT-bound AR (PDB code: 3L3X) chosen from RCSB Protein Data Bank (http://www.rcsb.org/pdb/home/home.do) was used as template. Quality of the achieved AR-LBD was evaluated with Ramachandran plot[11] (Figure S3) generated by the Structure Analysis and Verification Server (SAVES; http://services.mbi.ucla.edu/SAVES/).

Molecular docking was carried out by Surflex-Dock[12] program interfaced with SYBYL 7.3. Ligand binding cavity was found automatically in the AR-LBD. The optimized structures were then docked into the cavity under default settings. Generated ligand-receptor complexes were then used for molecular dynamics (MD) simulations.

Molecular dynamics simulations

MD simulations were performed using GROMACS 5.1.2[13,14] package on a Lenovo Flex System Blade cluster. CHARMM 27 force field[15] was employed to the proteins by GROMACS, and to the ligands by SwissParam[16] server (http://www.swissparam.ch/). The molecular system was immersed in a box filling with TIP3P[17] water molecules, and the distance between the complex and the boundary was kept at least 1.4 nm. System was then energy-minimized by use of the steepest-descent method, followed by 2 phases equilibration simulations under NVT (constant volume) and NPT (constant pressure) ensembles, respectively. MD simulations were performed with NPT ensemble under 1 bar pressure and 300 K for 16 ns or 10 ns. The Particle Mesh Ewald (PME) method was utilized for calculation of long-range electrostatic interactions. All bonds (even heavy atom-H bonds) were constrained using Linear Constraint Solver (LINCS).

Steered molecular dynamics simulations

Equilibrated conformation of each MD simulation was extracted for steered molecular dynamics (SMD) simulations. In SMD simulations, ligands were pulled out of the associating receptors along the chosen routes. The pulling force was applied (Equation S1)

$$F(t) = 2k(vt - x(t)) \quad \text{(S1)}$$

where k is the harmonic force constant for pulling ($\mathrm{kJ \cdot mol^{-1}nm^{-2}}$) and v is velocity (nm/ns) of the pulling force, while t and $x(t)$ are the simulation time (ns) and position of the ligand (nm) at time t. And the work W was calculated (Equation S2)

$$W(x(t)) = \int_0^{x(t)} F(t)\, dx(t) \quad \text{(S2)}$$

SMD simulations were also performed using GROMACS 5.1.2 package on a Lenovo Flex System Blade cluster. CHARMM 27 force field was employed to the proteins by GROMACS, and to the ligands by SwissParam server. System was then energy-minimized by use of the steepest-descent method, followed by equilibration simulations under NPT ensemble. Production MD simulations were conducted with NPT ensemble under 1 bar pressure and 300 K for 3 ns. A velocity of 1 nm/ns was used, and the harmonic force constant was set 1000 $\mathrm{kJ \cdot mol^{-1}nm^{-2}}$.

MM-PBSA binding free energy

MM-PBSA method[5] was used for binding free energy calculation after MD simulations. Generally, binding free energy $\Delta G_{binding}$ can be defined (Equation S3).

$$\Delta G_{binding} = G_{complex} - (G_{receptor} + G_{ligand}) \quad \text{(S3)}$$

where $G_{complex}$, $G_{receptor}$ and G_{ligand} are total free energies of the receptor-ligand complex, receptor, and ligand in solvent, respectively. The G value for each term (G_x) can be calculated (Equation S4).

$$G_x = E_{MM} - TS + G_{solvation} \quad \text{(S4)}$$

where E_{MM} is the molecular mechanics energy; TS denotes the entropic contribution where T and S refer to the temperature and entropy, respectively; $G_{solvation}$ is the solvation free energy.

Molecular mechanics energy E_{MM} includes the energy of bonded (E_{bonded}), electrostatic ($E_{electrostatic}$) and van der Waals (E_{vdW}) interactions (Equation S5).

$$E_{MM} = E_{bonded} + E_{electrostatic} + E_{vdW} \quad (S5)$$

Solvation free energy $G_{solvation}$ can be divided into two parts, electrostatic (G_{polar}) and nonelectrostatic ($G_{nonpolar}$) solvation free energy (Equation S6).

$$G_{solvation} = G_{polar} + G_{nonpolar} \quad (S6)$$

$G_{nonpolar}$ was calculated based on the solvent accessible surface area (SASA) model.

One hundred snapshots extracted from each MD trajectory were used for calculation of MM-PBSA binding free energy. All calculations of binding free energies were performed by use of the g_mmpbsa package[5] developed form GROMACS and APBS programs.

Data analyses

RMSD of MD trajectories were calculated using GROMACS. The average binding free energy was calculated using a bootstrap analysis by a Python script that was developed by Kumari et al [5]. The principal component analysis (PCA) of the binding and unbinding results were performed using the KNIME Analytics Platform version 3.3.2,[18] and the first component (LRI_{score}) was used to describe the ligand-AR interactions. The free energy decomposition was calculated by another Python script that was developed by Kumari et al [5]. The multi-linear regression for active antagonists was calculated using the KNIME Analytics Platform. Prior to regression, parameters were normalized using the z-score normalization method. Molecular descriptors were calculated by

RDKit packages on the KNIME Analytics Platform.

Supporting Discussions

Ligand unbinding

Several studies on nuclear receptors such as estrogen receptor (ER), glucocorticoid receptor (GR) and thyroid hormone receptor (TR) have demonstrated four major unbinding pathways,[19,20] which were depicted in Figure S6, A and B. Paths 1, 2 and 4 was strongly dependent on repositioning of H12. Therefore, based on conformations of BPs-AR, potential unbinding pathways of BPBP, BPC and BPPH were paths 1, 2 and 3, whereas those of other BPs were paths 3 and 4 (Table S2). Peaks of pulling forces (PFs) was used to compare the unbinding processes among BPs (Table 1 and Table S2). BPAP required the greatest PF (2.28×10^3 kJ/mol/nm) to dissociate from AR, whereas BPS required the least PF (4.93×10^2 kJ/mol/nm), followed by BPP, BPF and BPE (Table 1). Ligand dissociation has been considered to be an important feature for MD simulations of NRs.[21,22] For example, the "mousetrap" model, which imagines H12 as a lid for a supposed escaping pathway, was used to evaluate the unbinding of a ligand.[23] However, it provided a subjective comparison on a single pathway and remains controversial when considering more than one unbinding pathways. Pulling forces from SMD simulations indicated the major unbinding pathway of BPs and made the quantitative description possible.

Helix 12 reposition resulted in the coregulator recruitment patterns

Conformations of BPs-AR, FT-AR and DHT-AR complexes experienced fluctuations in different ranges during MD simulations, and the helix 12 (H12) experienced the most significant repositioning among all helixes and then became stable after approximately 8 ns (Figure S7). Three

modes, generally derived for all tested chemicals according to their repositioning of H12 were named modes A, B and S (Figure 1 and Table 1). H12 of mode A is in the active position, which blocks the CoR binding site and exposes the CoA binding site (Figure 1, A and B). H12 of mode B blocks both the CoA and CoR binding sites (Figure 1, A and C). H12 of mode S exposed both binding sites of CoA and CoR, which might lead to selective recruitment of CoA and CoR (Figure 1, A and D) [1]. As anticipated, H12 of DHT-AR equilibrated as mode A to inhibit CoR and recruit CoA, which agreed with results of coregulator recruitment assays and was consistent with crystal structures of DHT-ARs (Figure S8) and the agonistic effect of DHT.[24,25] The results of DHT-AR demonstrated the reliance of the MD simulations.

Workflow for MIE-based *in silico* screening

According to the mechanisms by which BPs initiated AR-mediated MIE at the functional and structural levels, this study developed a workflow for MIE-base *in silico* screening of endocrine disruptors. However, it should be noted that the MIE-based *in silico* screening should be considered to be a flexible tool that will always provide useful information in assessments of hazard, even though it will improve over time when new information on MIE and improved simulation methods are implemented [7]. Finally, as recommended by The Endocrine Society [26,27], more efforts should be made that focus on enzymes involved in hormone synthesis and metabolism, other than nuclear receptors, to provide more mechanistic insights into the screening of endocrine disrupting chemicals in the future.

Designing safer BPA substitute

Structures of BPs directly influenced their interaction with AR, which could aid in designing substitutes for BPA with no or lesser potential for disruption of AR-mediated pathways. BPs are

structurally similar compounds (Figure S2), with two phenol groups (PG1 and PG2; Figure S13) at their two ends, and a connecting group (CG; Figure S13) in the middle, which connects the two phenol groups. Differences in structures of BPs is mainly with CGs (except BPC and BPG). The BPs bound to AR in a similar binding mode (Figure S13). Generally, PG1s located in the seam between H3 and H6, where the hydroxyl on PG1s might form hydrogen bonds with residues Gln711, Met745 and Arg752. PG2s is bound to an area formed by H3, H6 and H11, which were more scattered than PG1s. CGs interacted mainly with residues on H8 and H11. By use of free energy decomposition, four residues (Met780, Met787, Phe876 and Leu880) on H8 and H11 were found to be the key residues (Table S4), consistent with the studies that have come to the same conclusion using point mutations [28,29]. Ligand-receptor interactions were found to correlate with free energy contributions of all four key residues (R^2=0.724, Figure S14), which meant that reducing the interactions between BPs and the residues would decrease the ligand-receptor interactions. Therefore, CGs contributed the most to the interaction between BPs and the 4 key residues on H8 and H11. Because Met780, Met787, Phe876 and Leu880 were hydrophobic residues, BPs of less hydrophobic and smaller CGs (Table S4) would result in weaker ligand-AR interactions. For example, due to its smaller size and because methyl is less hydrophobic than cyclohexyl, the methyl-CG BPF was less sufficient for interaction with the four residues than cyclohexyl-CG BPZ (Figure S13), which resulted in fewer ligand-receptor interactions of BPF. These findings revealed key interactions for ligand-receptor interactions and provided structural insights into BPA substitutes: smaller and less hydrophobic CGs would reduce the effect on AR.

Supporting Figures

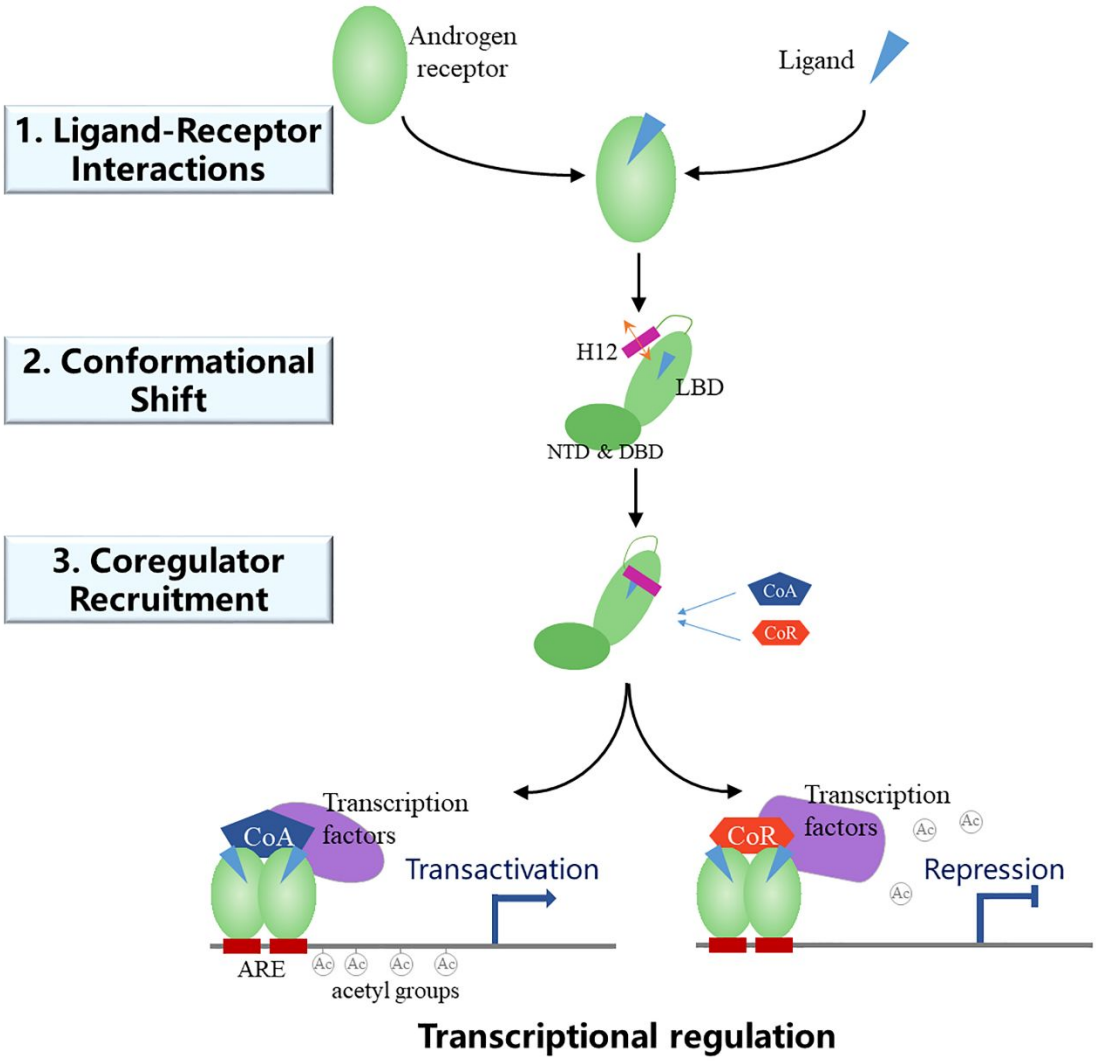

Figure S1. Key biochemical processes for an androgen receptor (AR) mediated molecular initiating event (MIE). NTD: amino-terminal domain; DBD: DNA binding domain; LBD: ligand binding domain; H12: helix 12; CoA: coactivator; CoR: corepressor; ARE: androgen response element.

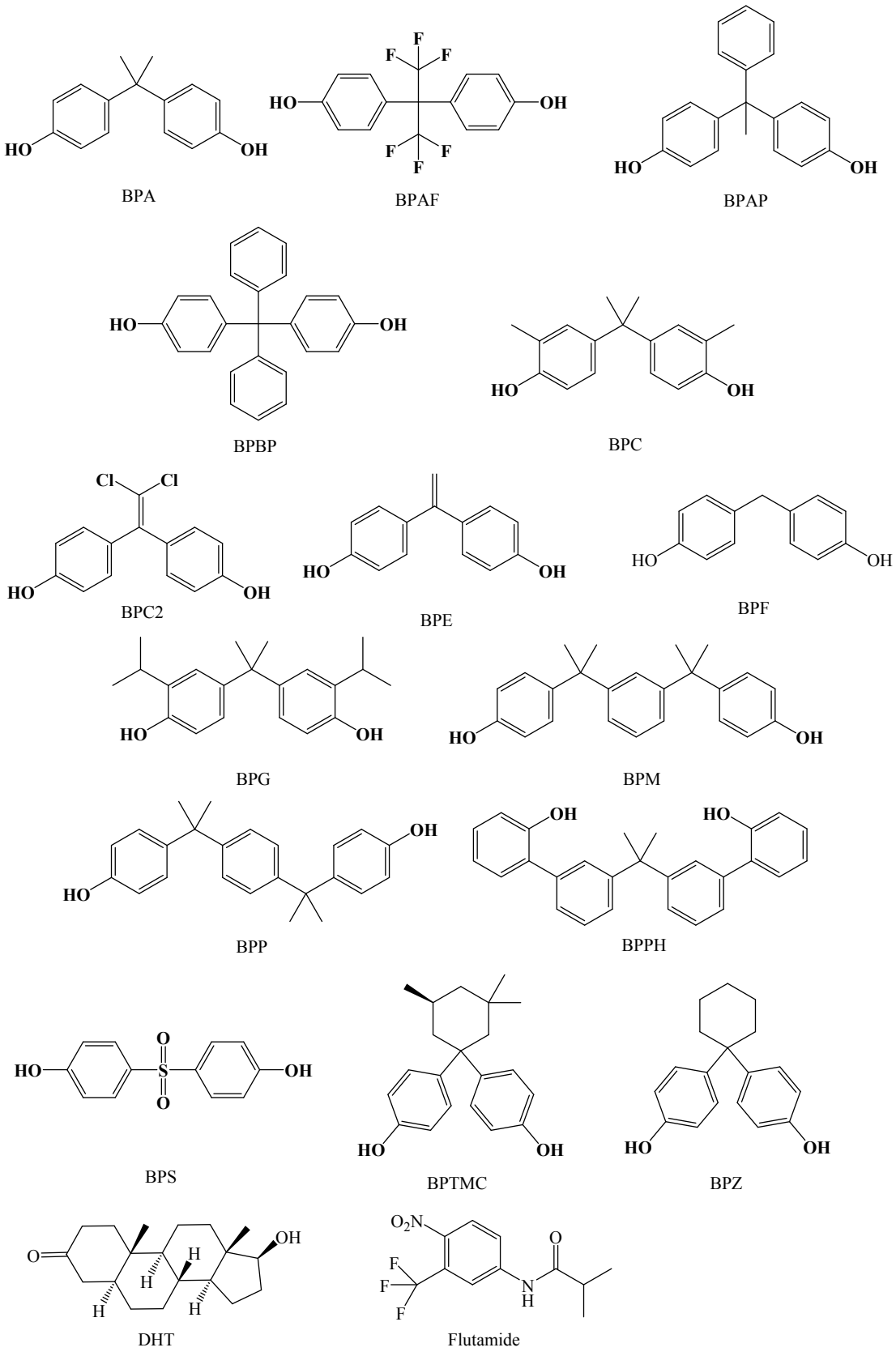

Figure S2. Molecular structures of bisphenols, DHT and flutamide used in the present study.

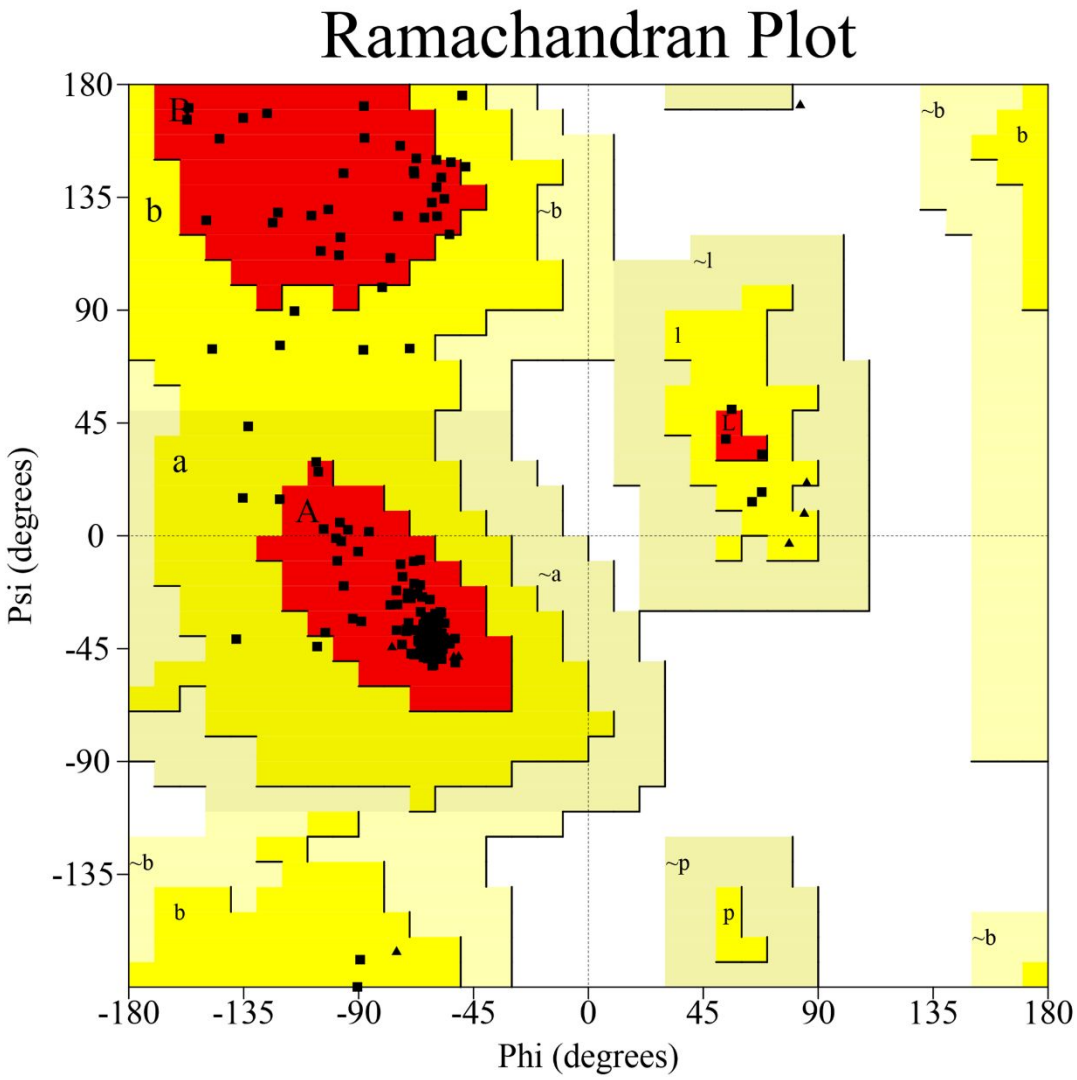

Figure S3. Ramachandran plot of the AR-LBD built by homology modeling. More than 90% of residues were in most favored regions, and no residues were in generously allowed or disallowed regions.

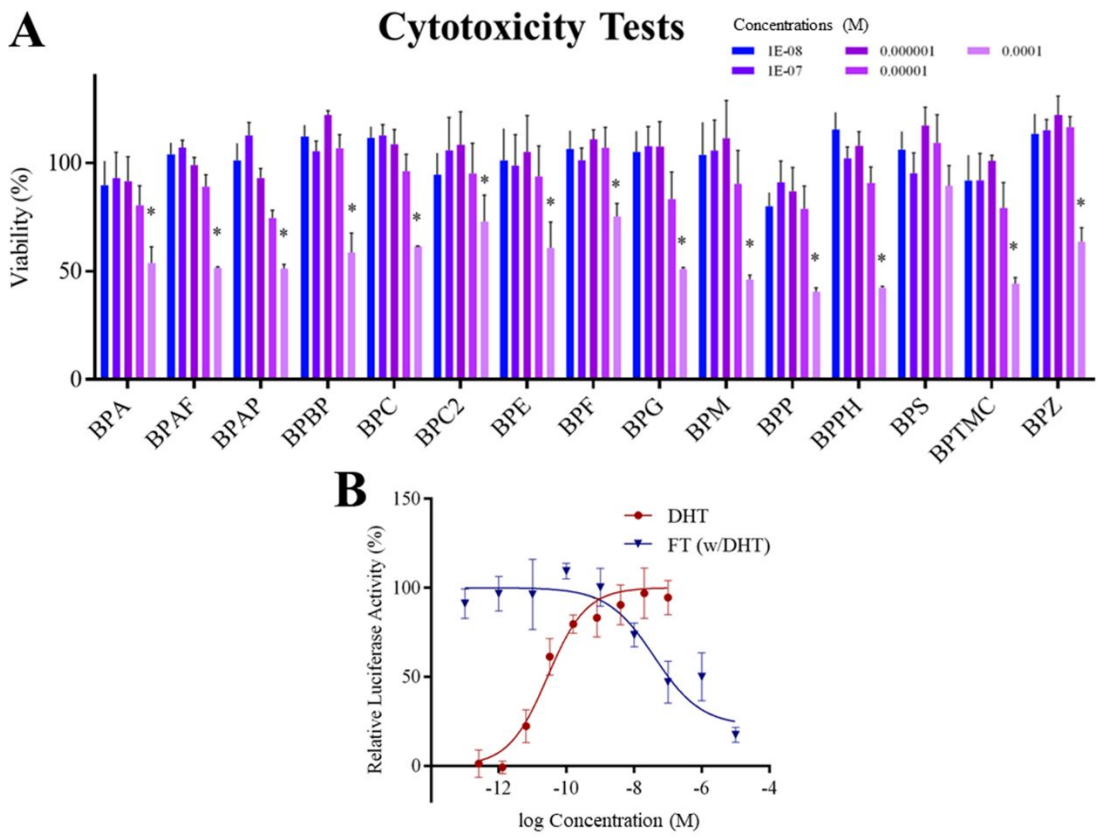

Figure S4. Results of reporter gene assays with the MDA-kb2 cell line. (A) Cytotoxicity tests for the bisphenols. Viability of solvent control (DMSO only) was defined as 100%. (B) Dose-responsive curves of 5α-dihydrotestosterone (DHT) and flutamide (FT, co-exposure with 1×10^{-9} M DHT), respectively. Relative luciferase activity of solvent control (DMSO only) was defined as 0%, while highest luciferase activity and luciferase activity of 1×10^{-9}M DHT exposure were defined as 100% for DHT and flutamide, respectively. Error bars represent standard error (SE) of at least three independent experiments. *$p < 0.05$ compared with 1×10^{-9}M DHT exposure.

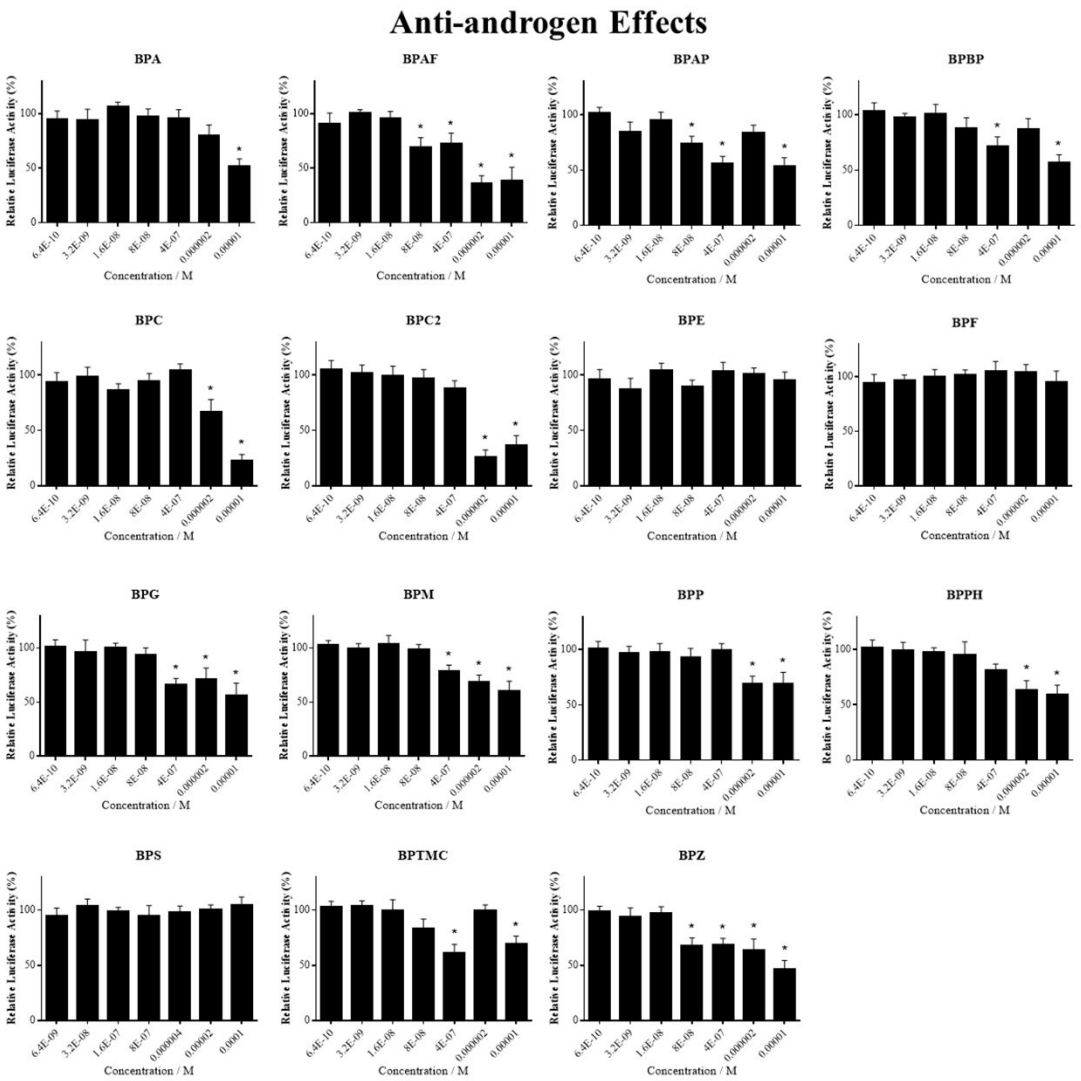

Figure S5. Results of the anti-androgenic effects of bisphenols. Cells were exposed to increasing doses of bisphenols with 1×10^{-9}M DHT. Relative luciferase activity of solvent control (DMSO only) was defined as 0%, while 1×10^{-9}M DHT exposure were defined as 100%. Error bars represent the standard error (SE) of at least three independent experiments. *$p < 0.05$ compared with 1×10^{-9}M DHT exposure.

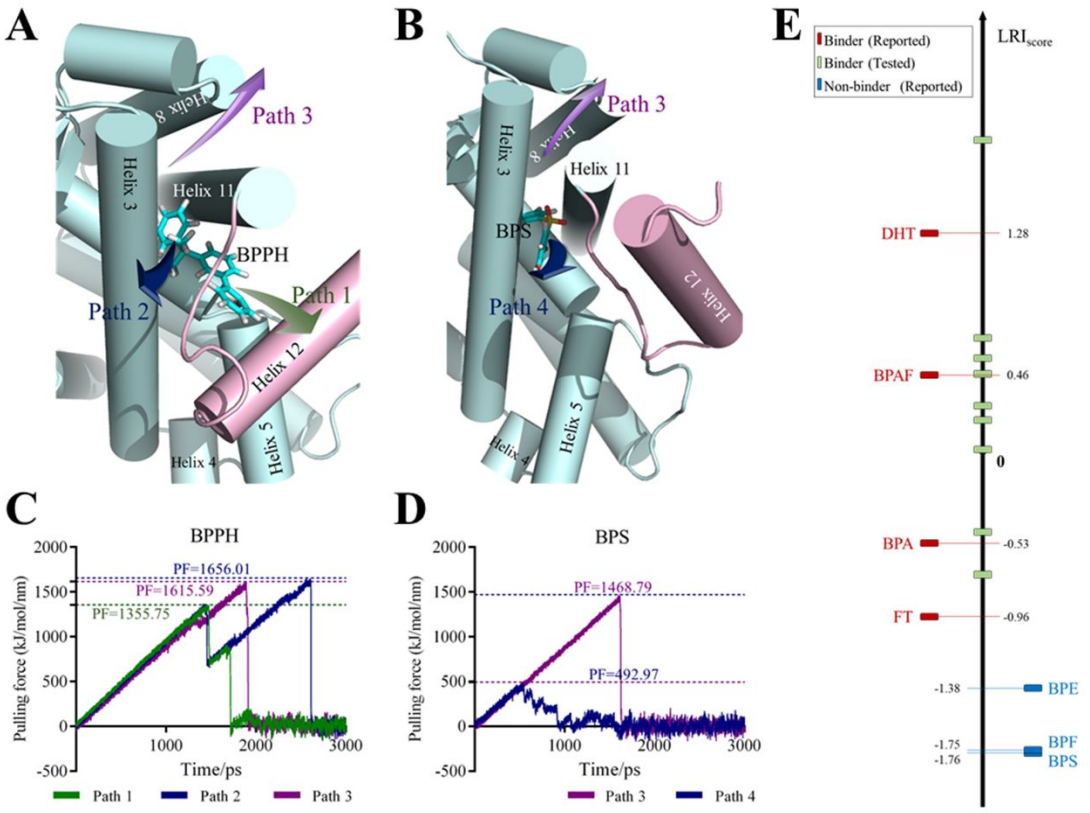

Figure S6. Unbinding of bisphenols from the androgen receptor (AR). (A, B) Unbinding pathways are represented by BPPH and BPS-bound AR, respectively. (C, D) Pulling force on BPPH and BPS, respectively, during the steered molecular dynamics simulations. The peaks of pulling forces (PFs, kJ/mol/nm) along different pathways are labeled. (E) Competitive binding results along ligand-receptor interaction score (LRI_{score}). Chemicals that have been reported as non-binders are colored blue, those reported as binders are colored red, and others that were determined as binders in this study are colored green.

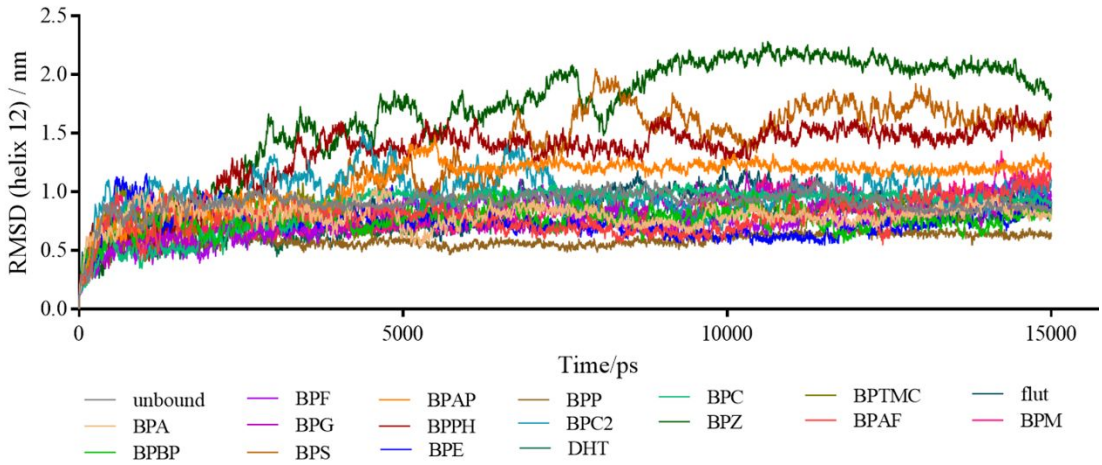

Figure S7. Root-mean-square deviation (RMSD) of helix 12 of ARs occupied by different ligands.

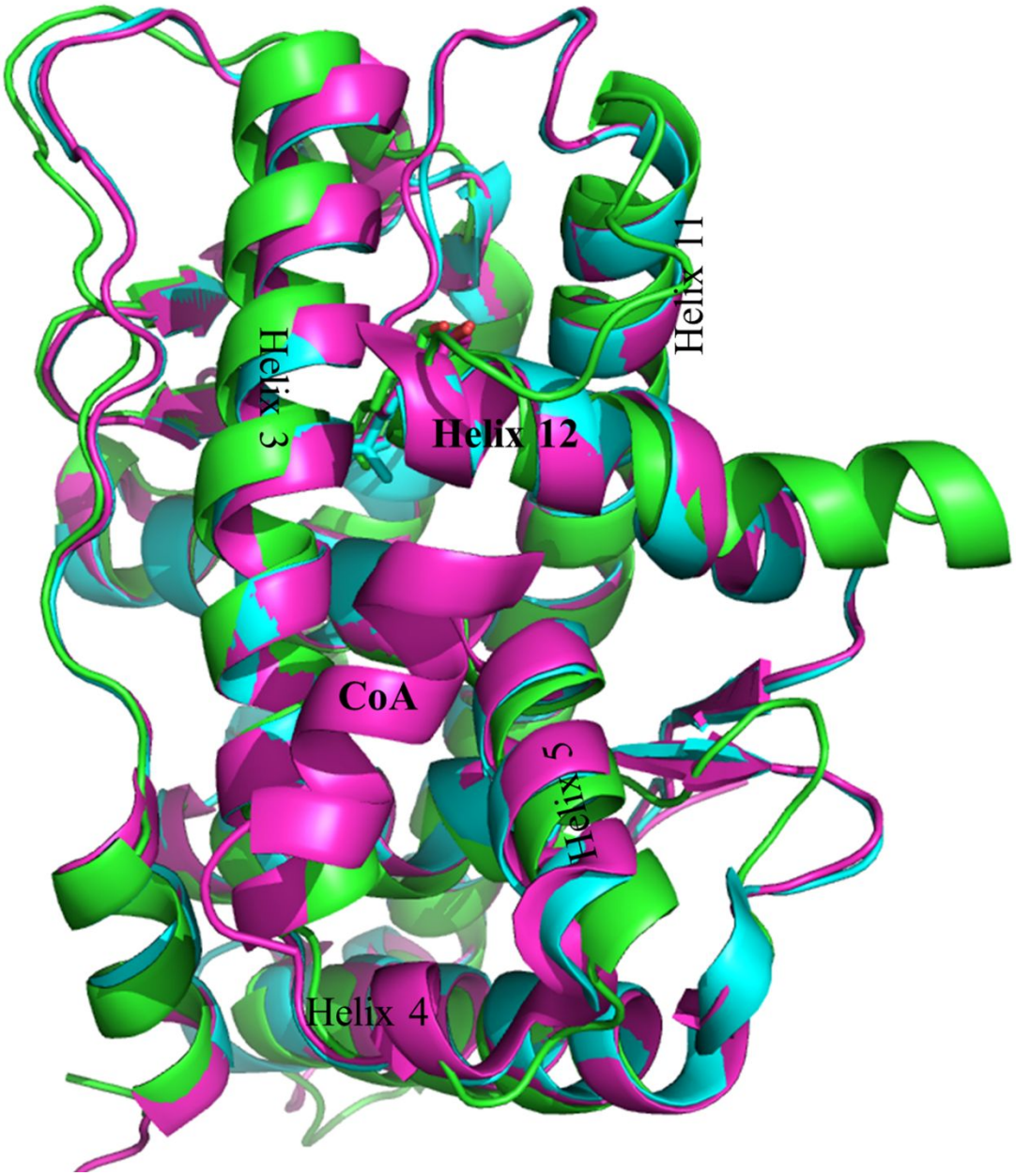

Figure S8. Conformations of DHT bound to ARs. Equilibrated conformation of DHT bound AR is colored green, while crystal structures encoded 1I37 and 3L3X from Protein Data Bank are colored cyan and hot-pink, respectively.

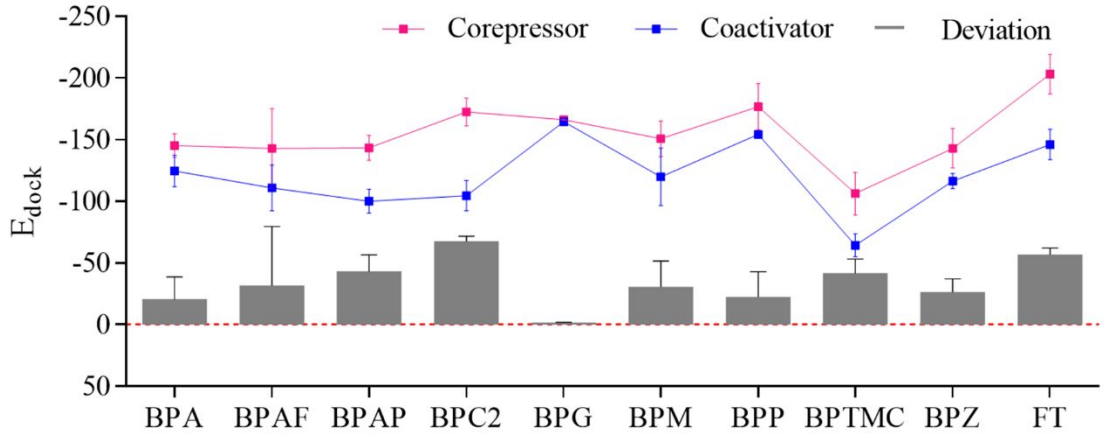

Figure S9. Docking score (E_{dock}) of the corepressor and the coactivator with ligand-bound ARs. Deviation is the difference of E_{dock} between the corepressor and the coactivator. The error bars refer to the standard deviation (SD) of three independent conformations.

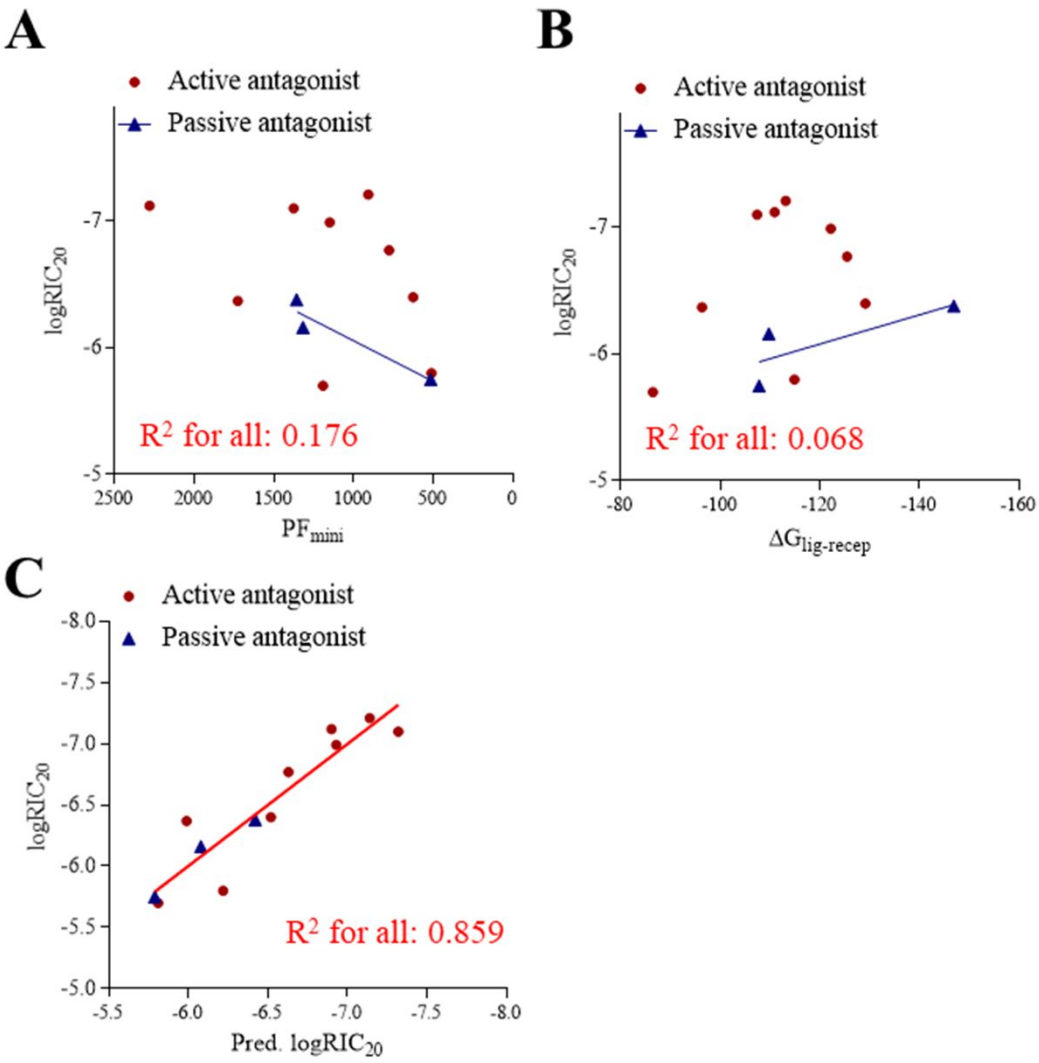

Figure S10. Plots of pulling force (A), binding free energy (B) and the predicted anti-androgenic potency (C) vs anti-androgenic potency from reporter gene assay.

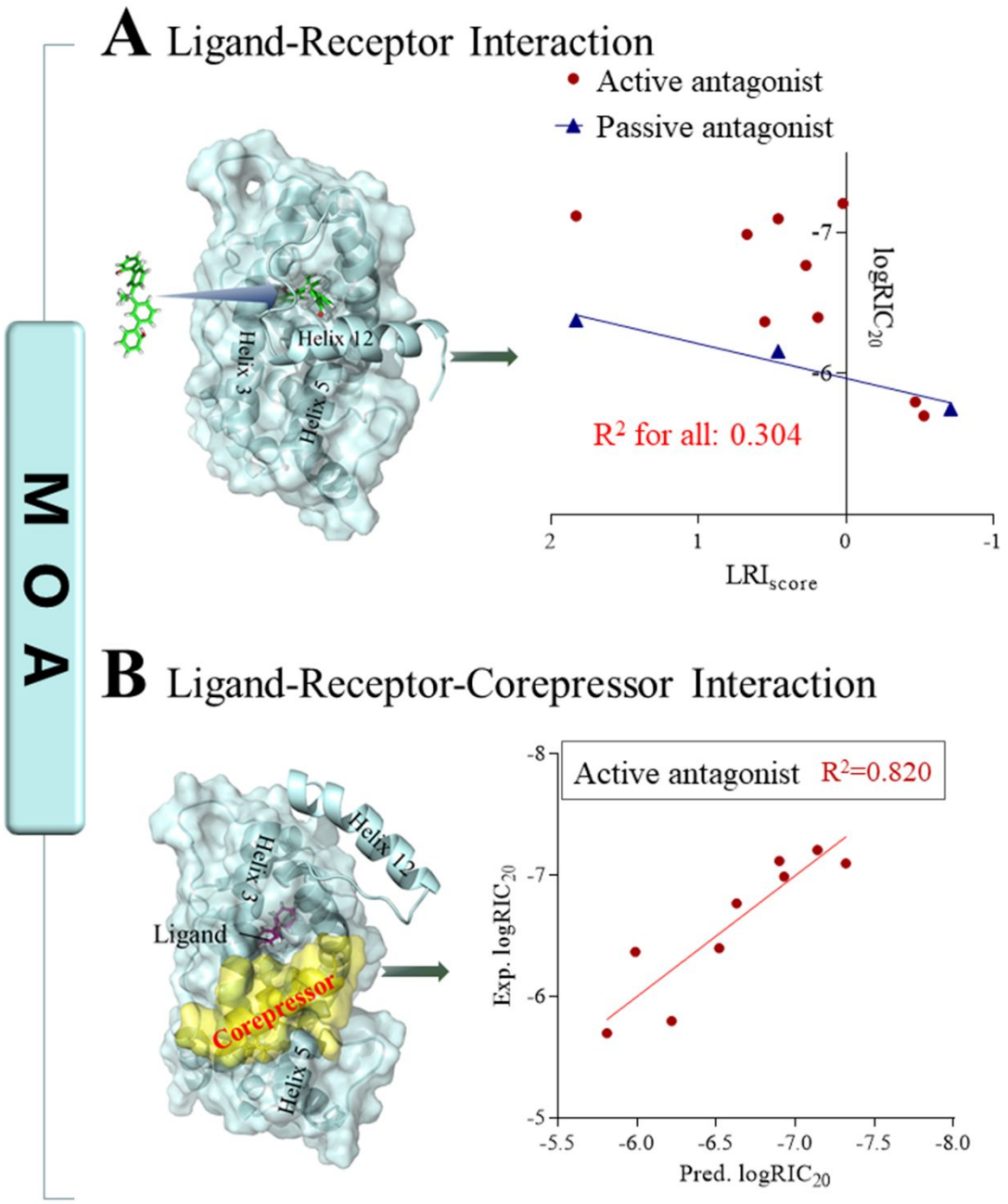

Figure S11. Predictions of anti-androgenic potencies under different mechanisms of action represented by ligand-receptor (A) and ligand-receptor-corepressor (B) interactions.

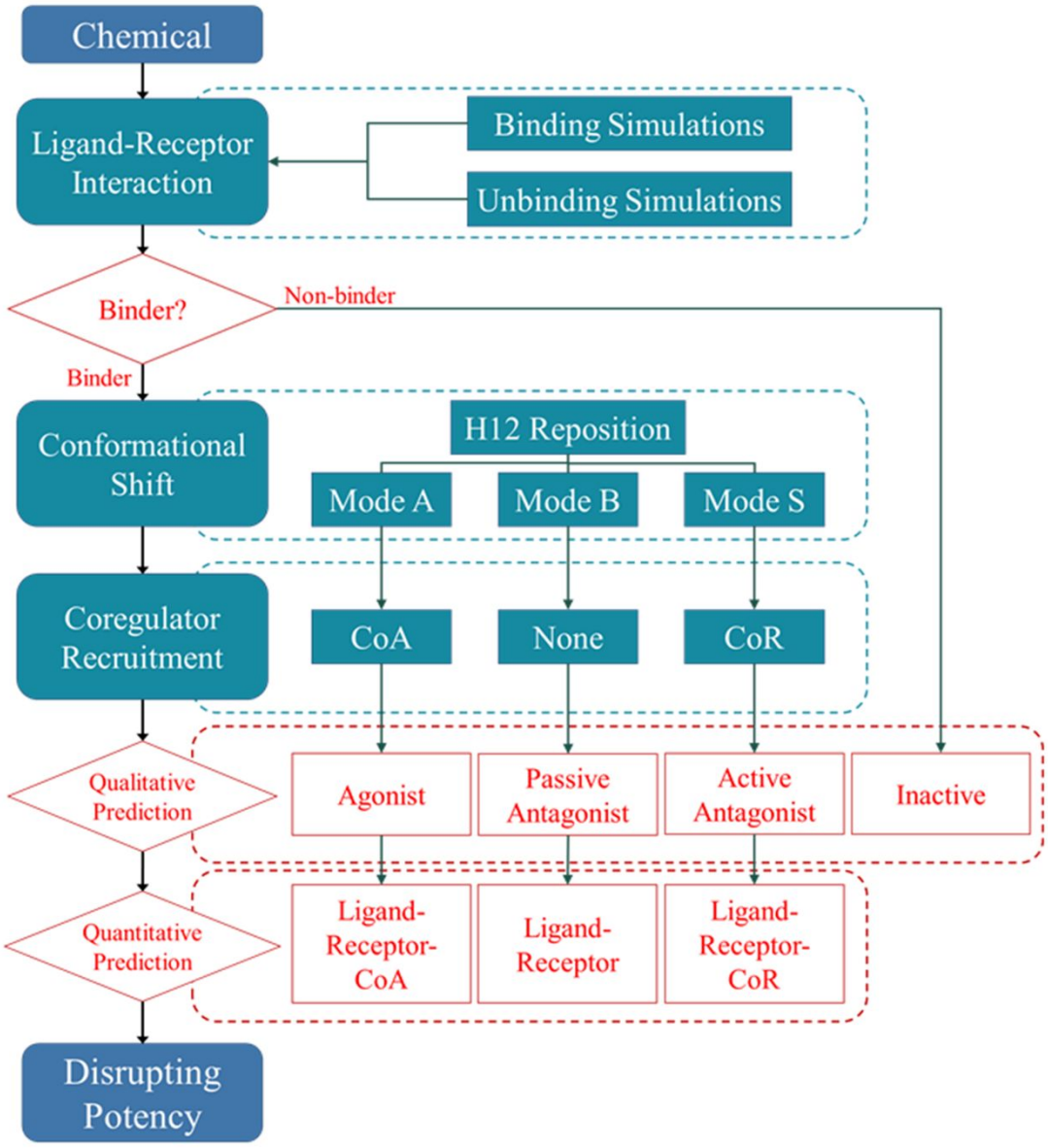

Figure S12. Workflow for molecular initiating event (MIE)-based *in silico* screening.

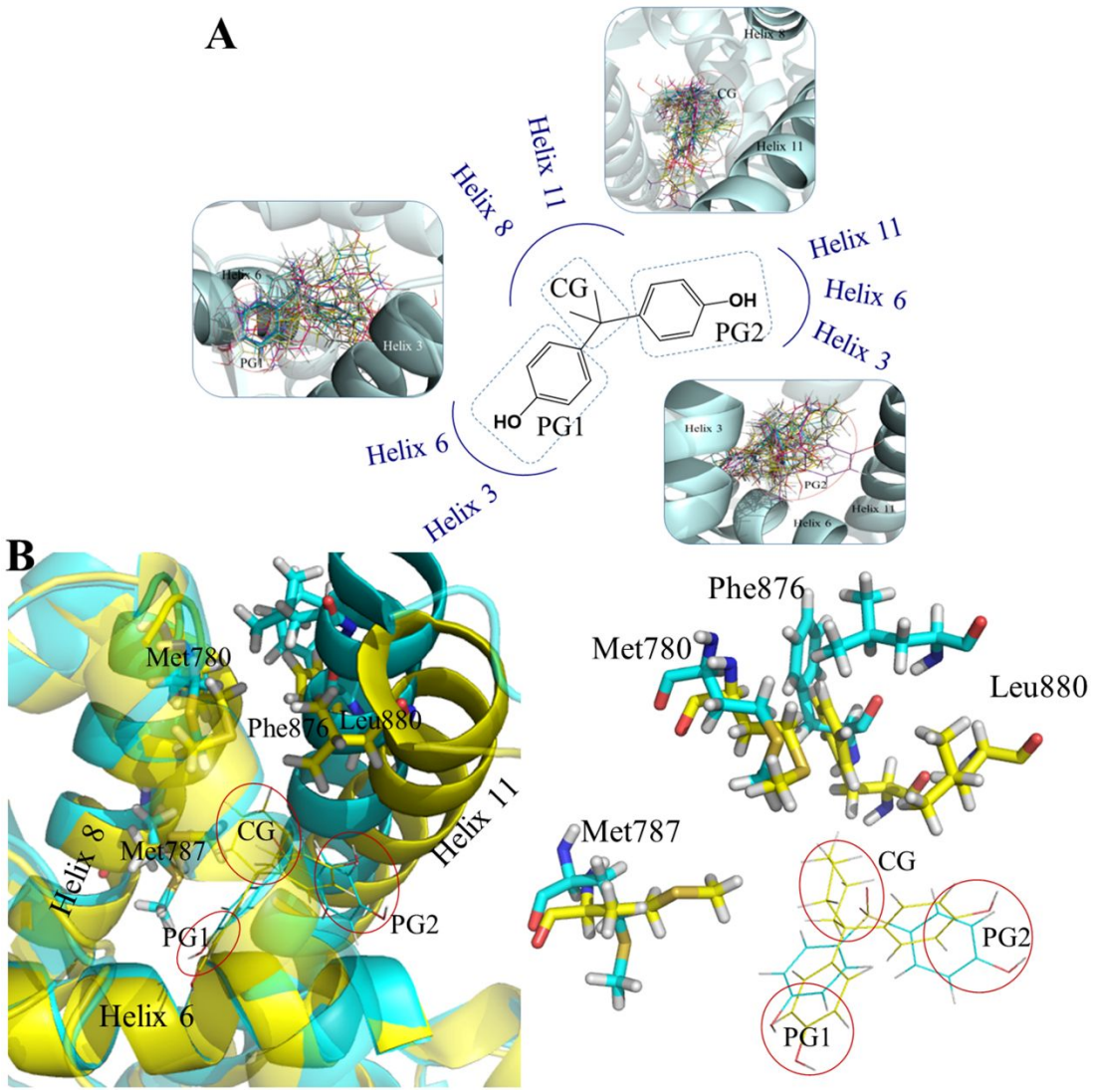

Figure S13. Structural features of bisphenols (BPs) and their interactions with androgen receptors (AR). (A) Connecting group (CG) and phenol groups (PG) and the general binding mode of BPs. (B) Specific groups and their interactions with key residues; ligands and key residues are extracted and shown on the right. Yellow and cyan represent BPZ-AR and BPF-AR complexes, respectively. Helixes, key residues and ligands are shown as cartoons, sticks and lines, respectively.

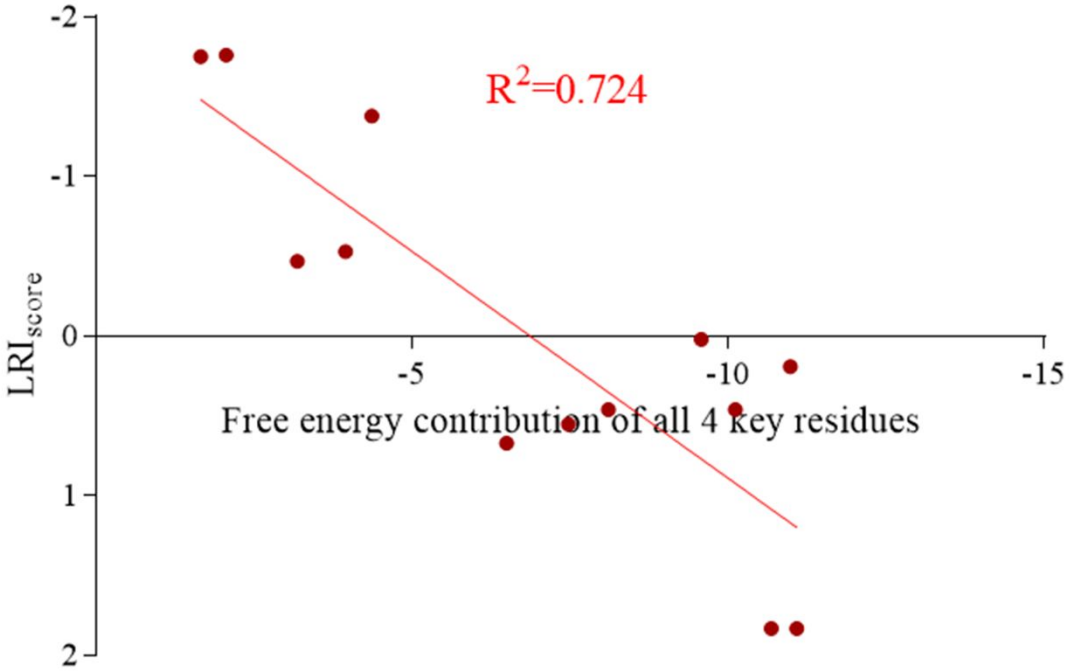

Figure S14. Plot of free energy contributions (kJ/mol) of all the 4 key residues versus LRI_{score}.

Supporting Tables

Table S1. Information of chemicals used in this study.

Chemical name	Abbreviation	CAS Number	Systematic name
Bisphenol A	BPA	80-05-7	2,2-Bis(4-hydroxyphenyl)propane
Bisphenol AP	BPAP	1571-75-1	1,1-Bis(4-hydroxyphenyl)-1-phenyl-ethane
Bisphenol AF	BPAF	1478-61-1	2,2-Bis(4-hydroxyphenyl)hexafluoropropane
Bisphenol BP	BPBP	1844-01-5	Bis-(4-hydroxyphenyl)diphenylmethane
Bisphenol C	BPC	79-97-0	2,2-Bis(3-methyl-4-hydroxyphenyl)propane
Bisphenol C 2	BPC2	14868-03-2	Bis(4-hydroxyphenyl)-2,2-dichlorethylene
Bisphenol E	BPE	2081-08-5	1,1-Bis(4-hydroxyphenyl)ethane
Bisphenol F	BPF	87139-40-0	Bis(4-hydroxyphenyl)methane
Bisphenol G	BPG	127-54-8	2,2-Bis(4-hydroxy-3-isopropyl-phenyl)propane
Bisphenol M	BPM	13595-25-0	1,3-Bis(2-(4-hydroxyphenyl)-2-propyl)benzene
Bisphenol S	BPS	80-09-1	Bis(4-hydroxyphenyl)sulfone
Bisphenol P	BPP	2167-51-3	1,4-Bis(2-(4-hydroxyphenyl)-2-propyl)benzene
Bisphenol PH	BPPH	24038-68-4	5,5’ -(1-Methylethyliden)-bis[1,1’-(bisphenyl)-2-ol]propane
Bisphenol TMC	BPTMC	129188-99-4	1,1-Bis(4-hydroyphenyl)-3,3,5-trimethyl-cyclohexane
Bisphenol Z	BPZ	843-55-0	1,1-Bis(4-hydroxyphenyl)-cyclohexane
Dihydrotestosterone	DHT	521-18-6	5α-Dihydrotestosterone
Flutamide	FT	13311-84-7	4'-Nitro-3'-trifluoromethylisobutyranilide

Table S2. Pulling forces along different pathways.

Chemical	path1	path2	path3	path4
BPA	NE	NE	1.60×10^3	1.19×10^3
BPAF	NE	NE	2.22×10^3	1.37×10^3
BPAP	NE	NE	2.31×10^3	2.28×10^3
BPBP	1.32×10^3	1.41×10^3	1.85×10^3	NE
BPC	6.35×10^2	5.16×10^2	6.45×10^2	NE
BPC2	NE	NE	1.97×10^3	1.73×10^3
BPE	NE	NE	9.20×10^2	5.13×10^2
BPF	NE	NE	2.09×10^3	5.11×10^2
BPG	NE	NE	Failed	7.76×10^2
BPM	NE	NE	1.72×10^3	6.24×10^2
BPP	NE	NE	2.40×10^3	5.10×10^2
BPPH	1.36×10^3	1.66×10^3	1.62×10^3	NE
BPS	NE	NE	1.47×10^3	4.93×10^2
BPTMC	NE	NE	Failed	1.15×10^3
BPZ	NE	NE	Failed	9.06×10^2
DHT	1.15×10^3	1.33×10^3	1.10×10^3	NE
FT	NE	NE	5.67×10^2	6.19×10^2

Peak pulling force (kJ/mol/nm) in each steered molecular dynamics (SMD) simulation along different pathway. NE: not exist. Failed: ligand failed to be pulled out within 3-ns SMD simulation.

Table S3. Results of molecular simulations of ligand-receptor-corepressor complexes and the prediction of anti-androgenic potencies.

Chemical	$\Delta G_{lig\text{-}recep/cor}$	$\Delta G_{cor\text{-}recep}$	PF_{path3}	PF_{path4}	PF_{mini}	LRI_{score}	$logRIC_{20}$	Predicted
BPA	-82.16	-165.99	1.71×10^3	6.42×10^2	6.42×10^2	-1.45	-5.70	-5.81
BPAF	-112.09	-260.88	Failed	1.43×10^3	1.43×10^3	0.69	-7.10	-7.32
BPAP	-109.24	-224.00	2.97×10^3	1.79×10^3	1.79×10^3	1.10	-7.12	-6.90
BPC2	-84.83	-165.80	1.61×10^3	1.55×10^3	1.55×10^3	-0.10	-6.37	-5.99
BPG	-126.54	-215.80	1.65×10^3	4.92×10^2	4.92×10^2	-0.08	-6.77	-6.63
BPM	-130.08	-201.51	1.11×10^3	7.82×10^2	7.82×10^2	0.44	-6.40	-6.52
BPP	-118.40	-176.97	2.65×10^3	1.11×10^3	1.11×10^3	0.48	-5.80	-6.22
BPTMC	-120.12	-226.92	Failed	1.46×10^3	1.46×10^3	1.03	-6.99	-6.93
BPZ	-110.52	-254.71	1.77×10^3	9.62×10^2	9.62×10^2	0.00	-7.21	-7.14

$\Delta G_{lig\text{-}recep/cor}$: binding free energies of ligands with AR/CoR (kJ/mol). $\Delta G_{cor\text{-}recep}$: binding free energies of CoR with ligand-bound AR (kJ/mol). PF_{pathx}: peak pulling force (kJ/mol/nm) in each steered molecular dynamics (SMD) simulation, PF_{mini} represents the minimum of different pulling paths. LRI_{score}: ligand-receptor interaction score. Failed: ligand failed to be pulled out within 3 ns SMD simulation. $LogRIC_{20}$: logarithm of the concentration (M) showing 20% inhibition of luciferase activity induced by 1×10^{-9}M DHT.

Table S4. Molecular descriptors and the free energy decomposition.

Chemical	MolWt	Volume	XLogP	LRI_{score}	Free energy contribution (kJ/mol)				
					Met780	Met787	Phe876	Leu880	All 4 res
BPA	228.12	223.25	4.52	-0.53	-1.33	-1.20	-0.69	-0.72	-3.94
BPAF	336.06	259.65	5.89	0.46	-2.86	-2.67	-1.52	-3.06	-10.11
BPAP	290.13	278.56	5.76	1.83	-2.85	-2.24	-2.38	-3.21	-10.68
BPBP	352.15	333.87	7.01	0.46	-3.14	-1.27	-1.86	-1.83	-8.10
BPC2	280.01	233.73	4.68	0.55	-1.36	-0.83	-2.89	-2.40	-7.47
BPE	212.08	203.31	4.01	-1.38	-1.45	-1.61	-0.61	-0.68	-4.36
BPF	200.08	188.65	3.18	-1.75	-0.42	-0.60	-0.24	-0.39	-1.65
BPM	346.19	347.74	7.83	0.19	-3.08	-2.65	-2.67	-2.58	-10.98
BPP	346.19	347.74	7.83	-0.47	-1.54	-0.71	-0.58	-0.36	-3.18
BPPH	380.18	368.47	8.40	1.83	-2.85	-3.14	-3.10	-1.99	-11.08
BPS	250.03	207.45	2.18	-1.76	-0.55	-0.67	-0.53	-0.30	-2.05
BPTMC	310.19	314.66	7.51	0.67	-2.52	-0.77	-2.21	-1.00	-6.49
BPZ	268.15	262.78	5.89	0.02	-2.48	-1.94	-2.00	-3.15	-9.57

MolWt: molecular weight; Volume: VABC Volume Descriptor; XlogP: predicted octanol/water partition coefficient. LRI_{score}: ligand-receptor interaction score.

References

(1) Chen, Q.; Tan, H.; Yu, H.; Shi, W. Activation of Steroid Hormone Receptors : Shed Light on the in Silico Evaluation of Endocrine Disrupting Chemicals. *Sci. Total Environ.* **2018**, *631–632*, 27–39.

(2) Gronemeyer, H.; Gustafsson, J. Å.; Laudet, V. Principles for Modulation of the Nuclear Receptor Superfamily. *Nat. Rev. Drug Discov.* **2004**, *3*, 950–964.

(3) Shiau, A. K.; Barstad, D.; Radek, J. T.; Meyers, M. J.; Nettles, K. W.; Katzenellenbogen, B. S.; Katzenellenbogen, J. A.; Agard, D. A.; Greene, G. L. Structural Characterization of a Subtype-Selective Ligand Reveals a Novel Mode of Estrogen Receptor Antagonism. *Nat. Struct. Biol.* **2002**, *9*, 359–364.

(4) Wilson, V. S.; Bobseine, K.; Lambright, C. R.; Gray, L. E. A Novel Cell Line, MDA-Kb2, That Stably Expresses an Androgen- and Glucocorticoid-Responsive Reporter for the Detection of Hormone Receptor Agonists and Antagonists. *Toxicol. Sci.* **2002**, *66*, 69–81.

(5) Kumari, R.; Kumar, R.; Lynn, A. G-Mmpbsa: A GROMACS Tool for High-Throughput MM-PBSA Calculations. *J. Chem. Inf. Model.* **2014**, *54*, 1951–1962.

(6) Baker, N. A.; Sept, D.; Joseph, S.; Holst, M. J.; McCammon, J. A. Electrostatics of Nanosystems: Application to Microtubules and the Ribosome. *Proc. Natl. Acad. Sci.* **2001**, *98*, 10037–10041.

(7) Chen, Q.; Wang, X.; Shi, W.; Yu, H.; Zhang, X.; Giesy, J. P. Identification of Thyroid Hormone Disruptors among HO-PBDEs: In Vitro Investigations and Coregulator Involved Simulations. *Environ. Sci. Technol.* **2016**, *50*, 12429–12438.

(8) Clark, M.; Cramer, R. D.; Van Opdenbosch, N. Validation of the General Purpose Tripos 5.2 Force Field. *J. Comput. Chem.* **1989**, *10*, 982–1012.

(9) Schwede, T.; Kopp, J.; Guex, N.; Peitsch, M. C. SWISS-MODEL: An Automated Protein Homology-Modeling Server. *Nucleic Acids Res.* **2003**, *31*, 3381–3385.

(10) Arnold, K.; Bordoli, L.; Kopp, J.; Schwede, T. The SWISS-MODEL Workspace: A Web-Based Environment for Protein Structure Homology Modelling. *Bioinformatics* **2006**, *22*, 195–201.

(11) Laskowski, R. A.; MacArthur, M. W.; Moss, D. S.; Thornton, J. M. PROCHECK: A Program to Check the Stereochemical Quality of Protein Structures. *J. Appl. Crystallogr.* **1993**, *26*, 283–291.

(12) Spitzer, R.; Jain, A. N. Surflex-Dock: Docking Benchmarks and Real-World Application. *J. Comput. Aided. Mol. Des.* **2012**, *26*, 687–699.

(13) Abraham, M. J.; Murtola, T.; Schulz, R.; Páll, S.; Smith, J. C.; Hess, B.; Lindah, E. Gromacs: High Performance Molecular Simulations through Multi-Level Parallelism from Laptops to Supercomputers. *SoftwareX* **2015**, *1–2*, 19–25.

(14) Pronk, S.; Pall, S.; Schulz, R.; Larsson, P.; Bjelkmar, P.; Apostolov, R.; Shirts, M. R.; Smith, J. C.; Kasson, P. M.; van der Spoel, D.; et al. GROMACS 4.5: A High-Throughput and Highly Parallel Open Source Molecular Simulation Toolkit. *Bioinformatics* **2013**, *29*, 845–854.

(15) MacKerell, A. D.; Bashford, D.; Bellott, M.; Dunbrack, R. L.; Evanseck, J. D.; Field, M. J.; Fischer, S.; Gao, J.; Guo, H.; Ha, S.; et al. All-Atom Empirical Potential for Molecular Modeling and Dynamics Studies of Proteins. *J. Phys. Chem. B* **1998**, *102*, 3586–3616.

(16) Zoete, V.; Cuendet, M. A.; Grosdidier, A.; Michielin, O. SwissParam: A Fast Force Field Generation Tool for Small Organic Molecules. *J. Comput. Chem.* **2011**, *32*, 2359–2368.

(17) Jorgensen, W. L.; Chandrasekhar, J.; Madura, J. D.; Impey, R. W.; Klein, M. L. Comparison of Simple Potential Functions for Simulating Liquid Water. *J. Chem. Phys.* **1983**, *79*, 926–935.

(18) Berthold, M. R.; Cebron, N.; Dill, F.; Gabriel, T. R.; Kötter, T.; Meinl, T.; Ohl, P.; Thiel, K.; Wiswedel, B. KNIME - the Konstanz Information Miner. *ACM SIGKDD Explor. Newsl.* **2009**, *11*, 26.

(19) Martínez, L.; Webb, P.; Polikarpov, I.; Skaf, M. S. Molecular Dynamics Simulations of Ligand Dissociation from Thyroid Hormone Receptors: Evidence of the Likeliest Escape Pathway and Its Implications for the Design of Novel Ligands. *J. Med. Chem.* **2006**, *49*, 23–26.

(20) Shen, J.; Li, W.; Liu, G.; Tang, Y.; Jiang, H. Computational Insights into the Mechanism of Ligand Unbinding and Selectivity of Estrogen Receptors. *J. Phys. Chem. B* **2009**, *113*, 10436–10444.

(21) Mackinnon, J. A. G.; Gallastegui, N.; Osguthorpe, D. J.; Hagler, A. T.; Estébanez-Perpiñá, E. Allosteric Mechanisms of Nuclear Receptors: Insights from Computational Simulations. *Mol. Cell. Endocrinol.* **2014**, *393*, 75–82.

(22) Wu, Y.; Doering, J. A.; Ma, Z.; Tang, S.; Liu, H.; Zhang, X.; Wang, X.; Yu, H. Identification of Androgen Receptor Antagonists: In Vitro Investigation and Classification Methodology for Flavonoid. *Chemosphere* **2016**, *158*, 72–79.

(23) Renaud, J. P.; Rochel, N.; Ruff, M.; Vivat, V.; Chambon, P.; Gronemeyer, H.; Moras, D. Crystal Structure of the RAR-Gamma Ligand-Binding Domain Bound to All-Trans Retinoic Acid. *Nature* **1995**, *378*, 681–689.

(24) Nadal, M.; Prekovic, S.; Gallastegui, N.; Helsen, C.; Abella, M.; Zielinska, K.; Gay, M.; Vilaseca, M.; Taulès, M.; Houtsmuller, A. B.; et al. Structure of the Homodimeric Androgen Receptor

Ligand-Binding Domain. *Nat. Commun.* **2017**, *8*, 14388.

(25) Zhou, X. E.; Suino-Powell, K. M.; Li, J.; He, Y.; MacKeigan, J. P.; Melcher, K.; Yong, E. L.; Xu, H. E. Identification of SRC3/AIB1 as a Preferred Coactivator for Hormone-Activated Androgen Receptor. *J. Biol. Chem.* **2010**, *285*, 9161–9171.

(26) Gore, A. C.; Chappell, V. A.; Fenton, S. E.; Flaws, J. A.; Nadal, A.; Prins, G. S.; Toppari, J.; Zoeller, R. T. EDC-2 : The Endocrine Society ' s Second Scientific Statement on Endocrine-Disrupting Chemicals. *Endocr. Rev.* **2016**, *36*, 1–150.

(27) Gore, A. C.; Chappell, V. A.; Fenton, S. E.; Flaws, J. A.; Nadal, A.; Prins, G. S.; Toppari, J.; Zoeller, R. T. Executive Summary to EDC-2: The Endocrine Society's Second Scientific Statement on Endocrine-Disrupting Chemicals. *Endocr. Rev.* **2015**, *36*, 593–602.

(28) Liu, H.; Han, R.; Li, J.; Liu, H.; Zheng, L. Molecular Mechanism of R-Bicalutamide Switching from Androgen Receptor Antagonist to Agonist Induced by Amino Acid Mutations Using Molecular Dynamics Simulations and Free Energy Calculation. *J. Comput. Aided. Mol. Des.* **2016**, *30*, 1189–1200.

(29) Bohl, C. E.; Wu, Z.; Miller, D. D.; Bell, C. E.; Dalton, J. T. Crystal Structure of the T877A Human Androgen Receptor Ligand-Binding Domain Complexed to Cyproterone Acetate Provides Insight for Ligand-Induced Conformational Changes and Structure-Based Drug Design. *J. Biol. Chem.* **2007**, *282*, 13648–13655.